Constraining properties of asymmetric dark matter candidates from gravitational-wave observations

Divya Singh[,1,*] Anuradha Gupta[,2] Emanuele Berti[,3] Sanjay Reddy[,4] and B. S. Sathyaprakash[1,5,6]

[1]*Department of Physics, Institute for Gravitation and the Cosmos,*
Pennsylvania State University, University Park, Pennsylvania 16802, USA
[2]*Department of Physics and Astronomy, The University of Mississippi, University, Mississippi 38677, USA*
[3]*Department of Physics and Astronomy, Johns Hopkins University,*
3400 North Charles Street, Baltimore, Maryland 21218, USA
[4]*Institute for Nuclear Theory, University of Washington, Seattle, Washington 98195, USA*
[5]*Department of Astronomy and Astrophysics, Pennsylvania State University,*
University Park, Pennsylvania 16802, USA
[6]*School of Physics and Astronomy, Cardiff University, Cardiff CF24 3AA, United Kingdom*

The accumulation of certain types of dark matter particles in neutron star cores due to accretion over long timescales can lead to the formation of a mini black hole. In this scenario, the neutron star is destabilized and implodes to form a black hole without significantly increasing its mass. When this process occurs in neutron stars in coalescing binaries, one or both stars might be converted to a black hole before they merge. Thus, in the mass range of ~ 1–$2M_\odot$, the Universe might contain three distinct populations of compact binaries: one containing only neutron stars, the second population of only black holes, and a third, mixed population consisting of a neutron star and a black hole. However, it is unlikely to have a mixed population as the various timescales allow for both neutron stars to remain or collapse within a short timescale. In this paper, we explore the capability of future gravitational-wave detector networks, including upgrades of Advanced LIGO and Virgo, and new facilities such as the Cosmic Explorer and Einstein Telescope (XG network), to discriminate between different populations by measuring the effective tidal deformability of the binary, which is zero for binary black holes but nonzero for binary neutron stars. Furthermore, we show that observing the relative abundances of the different populations can be used to infer the timescale for neutron stars to implode into black holes, and in turn, provide constraints on the particle nature of dark matter. The XG network will infer the implosion timescale to within an accuracy of 0.01 Gyr at 90% credible interval and determine the dark matter mass and interaction cross section to within a factor of 2 GeV and 10 cm^{-2}, respectively.

I. INTRODUCTION AND BACKGROUND

The origin and properties of dark matter (DM) have been long-standing problems in fundamental physics and cosmology. Astronomical observations have increasingly provided evidence for a nonbaryonic component of matter that either does not interact electromagnetically with baryons or has a negligibly small interaction cross section. Consequently, the presence of DM is inferred due to its gravitational effect on baryonic matter. Laboratory experiments to detect DM particles from their weak interaction with baryons have so far produced null results, as have the observations of decay products that would result from the annihilation of certain types of DM particles. Although there are a few plausible DM candidates in the Standard Model, theoretical insight into

what they might be in theories beyond the Standard Model is plentiful and not very constraining. Currently, there is an effort to look for DM over 60 orders of magnitude in mass, with candidates ranging from wavelike [1] and particle DM [2] to macroscopic objects such as primordial black holes (BHs) [3].

Observations of gravitational waves (GWs) by the Laser Interferometer Gravitational-Wave Observatory (LIGO) and Virgo over the past seven years [4–6] have opened up a new avenue for exploring DM. On the one hand, detecting BHs of unusually large masses (compared to astrophysical BHs observed until then) could hint at their primordial origin [7]. This remains a possibility, although several astrophysical models can account for the broad range of BH masses detected by LIGO and Virgo (see, e.g., [8,9]). The search for GWs from subsolar mass BHs has so far been unsuccessful, severely constraining the fraction of total DM content in primordial BHs [10,11]. If the Universe

[*]dus960@psu.edu

has no primordial BHs with masses of $\mathcal{O}(10 M_\odot)$, next-generation (XG) detectors can set upper limit on their abundance as a fraction of DM energy density as low as $f_{\mathrm{PBH}} \sim \mathcal{O}(10^{-5})$, about 2 orders of magnitude lower than current upper limits in this mass range; if instead $f_{\mathrm{PBH}} \gtrsim 10^{-4}$, future GW observations would exclude $f_{\mathrm{PBH}} = 0$ at the 95% credible interval [12]. The minimum testable abundance as a fraction of DM energy density depends on the primordial BH mass and can be as low as $f_{\mathrm{PBH}} \sim \mathcal{O}(10^{-10})$ (see, e.g., Fig. 5 of [13]).

An alternative way to constrain the presence of DM would be to look for its gravitational drag on the orbits of BHs and neutron stars (NSs) [14–24]. Additionally, the presence of an axionic cloud around BHs could extract the rotational energy from BHs, thereby affecting the spin distribution of BHs or producing continuous GWs from newly formed BHs [25,26]. Several authors have explored the prospect of making such observations [27–30]. In fact,

next-generation ground-based GW observatories, with the prospect of detecting several binary black hole (BBH) inspiral events each year with large signal-to-noise ratios (SNRs), could observe dozens of postmerger axionic signals [31], confirming or constraining bosons in the mass range $\sim[7 \times 10^{-14}, 2 \times 10^{-11}]$ eV [32].

In this paper, we explore the accumulation of bosonic asymmetric dark matter (ADM) in NS cores that could eventually form a stable mini BH, grow by Bondi-Hoyle accretion, and eventually lead NSs to implode and form BHs, without significantly changing their mass. Two plausible scenarios are described in Fig. 1. These mechanisms could be particularly efficient in regions of large DM densities, such as the central cores of large galaxies. It has been suggested that the lack of a sizable population of pulsars in the core of the Milky Way, where the density of DM is expected to be particularly high, is because most of them have imploded to form BHs [33]. While this
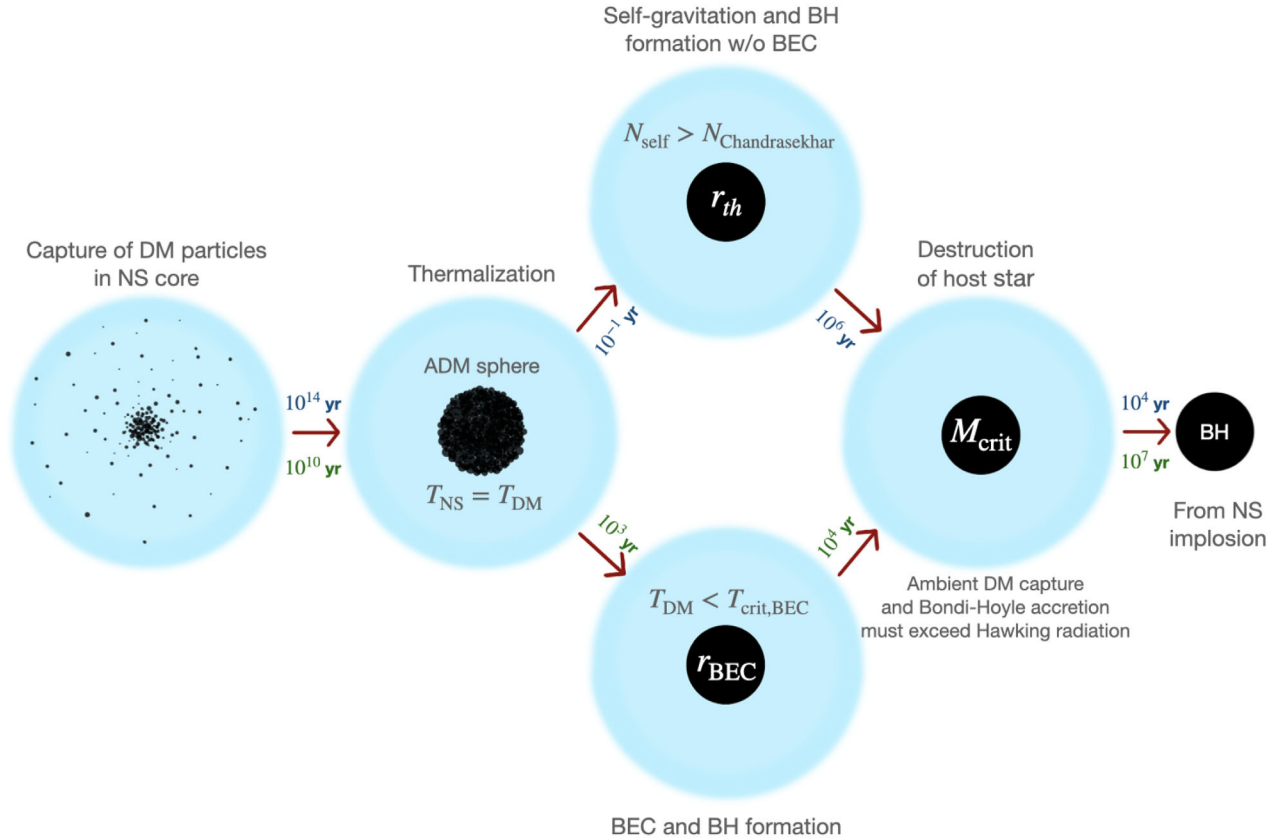

FIG. 1. Two plausible scenarios for the formation of BHs by imploding NSs without significantly changing their mass. In the first scenario, DM particles accumulate, thermalize, and form a self-gravitating object, which collapses to a BH if the number of DM particles exceeds the Chandrasekhar limit. In the second scenario, when a sufficiently large number of DM particles accumulates, a Bose-Einstein condensate (BEC) could form under favorable conditions and then collapse to a BH. Once a BH is assembled at the core, it can grow by accretion of NS matter, eventually leading to the implosion of the NS. The BH forms over a shorter timescale through BEC formation for DM particles of mass $m_\chi \leq 2 \times 10^4$ GeV. Therefore, we show the timescales with $m_\chi = 2 \times 10^4$ GeV for the channel where the BH forms without a BEC (blue) and with $m_\chi = 1$ GeV for the BEC channel (green), assuming a scattering cross section $\sigma_\chi = 2 \times 10^{-45}$ cm^{-2} and ambient DM density $\rho_\chi = 1$ GeV/cm^3.

explanation might not be the root cause of why the Galactic Center is deficient of pulsars, future GW observations could test if the implosion mechanism operates in NSs, as described below.

The timescale $t_c(\rho_\chi, m_\chi, \sigma_\chi)$ over which the accumulation of DM eventually makes NSs implode to form BHs depends on the DM density ρ_χ in the neighborhood of NSs, its mass m_χ, and its interaction cross section with hadrons σ_χ. NSs that live for a time longer than t_c will get converted to BHs, and those that live for a shorter duration will not. Although isolated NSs can last forever, those in a merging binary would only live for a time t_d, called the "delay time," before they inspiral and merge to either form (rarely) supermassive NSs or (frequently) BHs. The delay time depends on the companion masses and the periapsis and eccentricity of the binary at the time when it first forms. The delay time, therefore, is not the same for all binary neutron stars (BNSs). Instead, the NS binary population is characterized by a certain delay-time distribution $P(t_d)$.

The probability distribution $P(t_d)$ is not well known, but it is often assumed to scale like $P(t_d) \propto 1/t_d$ [34–38]. The fraction of the population for which $t_d > t_c$ will be converted to BHs and the rest will remain as NSs. For the population of mergers detected with a sufficiently large SNR, GW observations can determine the fraction of the BNS population that has been converted to BBHs. This fraction, if nonzero, can be used to infer the implosion timescale $t_c(\rho_\chi, m_\chi, \sigma_\chi)$ and hence constrain the parameter space of local DM density, DM mass, and interaction cross section. If the population does not contain any BBHs, then it will be possible to set limits on the very same quantities.

It is quite possible, although unlikely, that BHs in the mass range of NSs of $1 - 3M_\odot$ are produced by stellar evolution or, alternatively, they could be primordial in origin [39,40]. The current consensus is that massive stars up to $\sim 23M_\odot$ leave behind NSs of masses in the range $1.2 - 2.0M_\odot$ at the end of their lives, while more massive stars are likely to leave behind a BH of mass greater than about $\sim 5M_\odot$ [41–45]. Although the primordial Universe could produce BHs in the mass range of NSs, they should also produce subsolar mass BHs. A detection of subsolar mass BHs could hint at the early Universe origin of BHs with NS masses. Moreover, primordial BHs are expected to have small spin magnitudes if they do not increase their spin by coherent accretion [46], while BHs formed from imploding NSs could have nonzero spins (see, e.g., [47,48]). Consequently, it might be possible to discriminate between the two populations from their spin distributions [49]. Another proposal to distinguish primordial BHs from astrophysical compact objects is to use their mass distribution and the redshift evolution of the merger rates by using LIGO-Virgo-KAGRA and A+ detections of the stochastic GW background [50] and possibly (in the future) Cosmic Explorer and Einstein Telescope observations of the stochastic background produced by subsolar mass compact objects [51].

The above argument assumes that either both NSs will implode, or neither does. If the time difference between the formation of the two NSs is large compared to the delay time t_d, then it is possible that only one of the NSs gets converted to a BH, but not its companion. However, this scenario is likely to be very rare.

The complex evolutionary process leading to NS formation is not completely understood, but stellar evolution models broadly suggest that NSs form from progenitors whose mass M lies in the range $8M_\odot \lesssim M \lesssim 23M_\odot$ [45]. The lifetime of such progenitor stars in the main sequence, which varies as $10(M/M_\odot)^{-2.5}$ Gyr [52], would be in the range 4–55 Myr. The heavier companion would evolve through the main sequence (MS) first to form a NS, followed by the lighter progenitor after a delay $\Delta t_{\rm MS}$. Assuming that the progenitors are drawn from the Salpeter mass function, i.e., $P(m) \propto m^{-2.3}$ [53], we find that $\Delta t_{\rm MS}$ has a median value of ~ 14 Myr, which is smaller than the smallest delay time $t_d^{\rm min} = 20$ Myr that we will be using in this work, and likely much smaller than the implosion timescale t_c, which could be as large as billions of years. A specific binary with delay time t_d will be seen as a BBH if $t_c < t_d$, as a BNS if $t_c > t_d + \Delta t_{\rm MS}$, or as a neutron star–black hole (NSBH) system otherwise. In Fig. 2 we plot the three fractions, and we see that the NSBH population constitutes at best about 6% of the total, and only over a small range of values of t_c. Consequently, we can safely assume that either both NSs in a binary would implode to form BHs, or neither would.

Observations of GWs could potentially discriminate the BBH population from that of BNSs. In the final moments before a BNS coalesces, each star experiences the tidal field of its companion, inducing a time-varying quadrupole deformation and associated emission of GWs. This is a
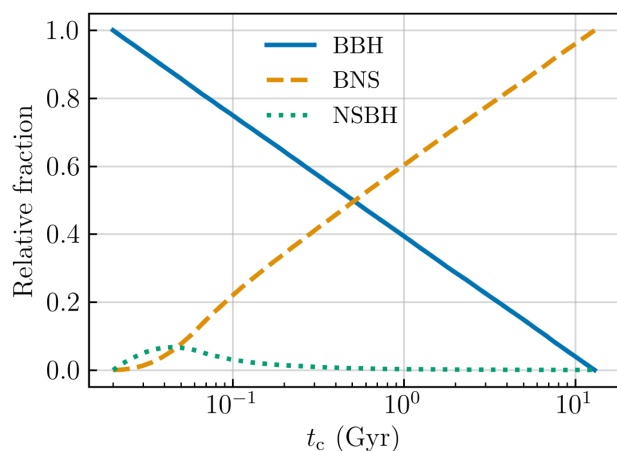

FIG. 2. The fraction of BBH and NSBH binaries formed from the implosion of one or both NSs, compared to the fraction of BNS systems as a function of the implosion timescale t_c. As a function of t_c the NSBH fraction remains negligibly small and can be ignored.

high-order post-Newtonian effect—technically a fifth post-Newtonian effect or a $(v/c)^{10}$ correction in the orbital phase evolution of the binary, where v is the orbital speed and c is the speed of light [54,55]—which becomes important before the two NSs merge with each other and will be absent in the case of BBHs [56–59]. Thus, by measuring the "tidal polarizability," often referred to as the "effective tidal deformability," it will be possible to ascertain the fraction of the two populations. It will not be possible to measure tidal deformability with sufficiently good accuracy for the entire observed population, but only for a fraction with sufficiently large SNR. In this paper we explore the sensitivity of future ground-based GW detectors to constrain the properties of a class of DM particles that can accumulate in NS cores and cause implosion, given sufficiently large time.

The rest of the paper is organized as follows. In Sec. II, we recall how tidal effects are encoded in GWs from BNSs. In Sec. III, we introduce the various GW detector networks and the waveform model used in this study and compute the accuracy with which the tidal deformability of a BNS can be measured using the Fisher matrix formalism. This will be followed by a computation in Sec. IV of the relative rates of BBHs and BNSs, as a function of the unknown implosion timescale t_c needed to form this novel population of BBHs. It turns out that the most important hyper-parameter needed in the computation of relative rates is the implosion timescale t_c. Thus, from the measured relative rates we can infer the implosion timescale, as shown in Sec. V. In Sec. VI, we discuss the physics of implosion from DM accretion and the various timescales involved in the problem, from accumulation of DM particles to form a mini-BH, through self-gravitation with or without the formation of a Bose-Einstein condensate, its growth, and the final implosion of the NS (cf. Fig. 1). In Sec. VII, we derive the constraints that can be placed on DM particles if the proposed analysis does not find a single BBH event in the mass range of $1 - 3M_\odot$ (which would imply that the implosion timescale is larger than the Hubble time) and obtain the properties of bosonic DM particles assuming a collapse time of 1 Gyr. In Sec. VIII, we briefly summarize our findings, as well as our plans to apply this technique to the known population of LIGO-Virgo binary mergers for a number of implosion scenarios and different DM candidates. In the Appendix we discuss how variations in the "true" collapse time affect the inferred bounds.

II. TIDAL INTERACTION TO DISTINGUISH BINARY NEUTRON STARS FROM BINARY BLACK HOLES

In this section we will discuss how to distinguish BNS mergers from BBH mergers using GW observations. An important difference in the GWs from the coalescence of BBH and BNS systems is that waves from BNS mergers have imprinted in them the tidal interaction between the

two bodies, while BBH mergers will have no such signature [56,60]. Additionally, while BBH mergers leave behind a BH remnant, BNS mergers could either promptly form a BH or leave behind a long-lived NS remnant with neutron-rich relativistic ejecta and a thermonuclear fireball. In this work, we will only consider the tidal interaction between the two bodies during the adiabatic inspiral regime. A merger accompanied by an electromagnetic afterglow essentially rules out a BBH merger.

A. Tidal deformability

A massive body produces a tidal field. The deformation induced by the tidal field on other bodies can be expressed as a multipole expansion, the quadrupole being the dominant multipole. Consider a spherically symmetric NS of radius R in the tidal field $\mathcal{E}_{ij}$ of its companion NS. The quadrupole deformation Q_{ij} induced in the star is related to the tidal field via the tidal deformability as

$$Q_{ij} = -\lambda \mathcal{E}_{ij}, \tag{1}$$

where $\lambda \equiv -\frac{2}{3G} k_2 R^5$, R is the star's radius, and k_2 is the dimensionless tidal Love number. The tidal Love number, which measures a body's rigidity, depends on the equation of state (EOS) of the NS via its compactness $C \equiv Gm/(c^2 R)$, where m is the mass of the star [61]. For NS equations of state considered in this paper, we have $k_2 \sim 0.1$ [62].

In a binary system of stars orbiting each other, the above quadrupole deformation is a function of time, which generates gravitational radiation, modifying the emitted signal at the fifth post-Newtonian order, inducing a $(v/c)^{10}$ correction to the dynamics of the system beyond the dominant quadrupole radiation reaction. In other words, the tidal interaction dissipates additional orbital energy into GWs, thus changing the orbital phase evolution of the waves at $(v/c)^{10}$ order beyond the quadrupole. This modification is significant in the final few cycles of the inspiral and coalescence of a binary and can be detected if the signal is observed with a high SNR.

The tidal deformability λ has dimensions of kg m² s², but what appears in the post-Newtonian dynamics is the dimensionless tidal deformability, defined by

$$\Lambda \equiv \frac{c^{10}\lambda}{G^4 m^5} = \frac{2}{3} k_2 C^{-5}. \tag{2}$$

As mentioned before, the Love number k_2 generally decreases with increasing compactness, thus the tidal deformability falls of steeper than C^{-5}. For candidate equations of state of NSs Λ decreases with the NS's mass and varies over the range $\sim[100, 4000]$ for NS masses in the range $1.1 - 1.5M_\odot$ considered in this study (see, e.g., Fig. 1 of Ref. [63]), the smallest values corresponding to largest NS masses and softer equations of state, and largest values corresponding to smallest masses and stiffer

equations of state. For BHs, $\Lambda = 0$ [56–58]: this is the key to distinguishing BBH mergers from NSBH and BNS mergers [64–66].

B. Tidal signature in neutron star binary signal

The GWs produced by BNSs are accurately described by post-Newtonian theory. We assume NSs have negligibly small spins and are on quasicircular orbits. These are reasonable assumptions, as companions in Galactic double NS systems have negligible spins (based on Ref. [67], see also Fig. 2.17 of Ref. [68]) and gravitational radiation backreaction causes orbital eccentricity to decay more rapidly compared to the orbital separation [69]. In the Fourier domain, the strain amplitude $\tilde{h}(f)$ measured by an interferometric GW detector in response to an incident BNS signal on a quasicircular orbit is given by

$$f\tilde{h}(f) = \mathcal{A}(f)e^{i\psi_{\text{PP}}(f)+i\psi_{\text{Tidal}}(f)}, \qquad (3)$$

where ψ_{PP} and ψ_{Tidal} are contributions to the Fourier phase from the point-particle approximation and tidal effects, respectively, and a factor of f is included to make the right-hand side dimensionless. The amplitude $\mathcal{A}(f)$ and the phase $\psi_{\text{PP}}(f)$ are given by [70]

$$\mathcal{A}(f) = \sqrt{\frac{5\nu}{6}} \frac{M}{D_{\text{eff}}} (\pi M f)^{-1/6}, \qquad (4)$$

$$\psi_{\text{PP}}(f) = \frac{5}{128\nu} \sum_{k=-5}^{2} \left[\alpha_k + \alpha_{kl} \log \frac{v}{v_0}\right] (\pi M f)^{k/3}, \qquad (5)$$

$$D_{\text{eff}} = \frac{4D_L}{\sqrt{F_+^2(1+\cos^2\iota)^2 + 4F_\times^2 \cos\iota}}. \qquad (6)$$

Here $M \equiv m_1 + m_2$ is the binary's total mass, m_1 and m_2 are masses of the companion stars, $F_+(\theta,\phi,\psi)$ and $F_\times(\theta,\phi,\psi)$ are the detector antenna pattern functions [see, e.g., [71]], D_L is the luminosity distance to the source, $D_{\text{eff}} > D_L$ is the effective distance, (θ,ϕ) describe the position of the source in the sky, ι is the angle between the line sight to the binary and the orbital angular momentum, and ψ is the polarization angle. The post-Newtonian coefficients α_k and α_{kl} depend on the symmetric mass ratio $\nu \equiv m_1 m_2/M^2$, except for the log terms in the post-Newtonian expansion and the tidal terms, which do depend on the total mass. The post-Newtonian expansion is carried out in powers of v/c, where $v = (\pi M f)^{1/3}$, and f is the GW frequency. Relative to the dominant quadrupole term, the tidal terms occur at the fifth post-Newtonian order and higher, i.e., a $(v/c)^{10}$ effect or, equivalently, $(\pi M f)^{10/3}$ term in the Fourier phase in Eq. (4) relative to the dominant term [72]. The dominant tidal contribution to the phase and the first post-Newtonian corrections are (see, e.g., [73])

$$\psi_{\text{Tidal}}(f) = -\frac{39}{2}\tilde{\Lambda}v^{10} + \left(\frac{6595}{364}\delta\tilde{\Lambda} - \frac{3115}{64}\tilde{\Lambda}\right)v^{12}. \qquad (7)$$

The dominant tidal term at the fifth post-Newtonian order depends on the mass ratio-weighted sum of the individual tidal deformabilities, defined as

$$\tilde{\Lambda} = \frac{1}{26}\left[(1+12q)\Lambda_1 + \left(1 + \frac{12}{q}\right)\Lambda_2\right], \qquad (8a)$$

while the correction at the sixth post-Newtonian order depends on $\tilde{\Lambda}$ as well as the difference in the tidal deformabilities, given by

$$\delta\tilde{\Lambda} = \sqrt{1-4\nu}\left(1 - \frac{13272}{1319}\nu + \frac{8944}{1319}\nu^2\right)\frac{(\Lambda_2 + \Lambda_1)}{2}$$
$$+ \left(1 - \frac{15910}{1319}\nu + \frac{32850}{1319}\nu^2 + \frac{3380}{1319}\nu^3\right)\frac{(\Lambda_2 - \Lambda_1)}{2}. \qquad (8b)$$

Note that, for NSs of comparable masses, i.e., $\nu \simeq 1/4$, we have $\Lambda_1 \simeq \Lambda_2$, $\tilde{\Lambda} \simeq \Lambda_{1,2}$, and $\delta\tilde{\Lambda} \simeq 0$. Thus, the second term is not only a subdominant post-Newtonian effect—the expansion coefficient is itself small for most BNSs. Therefore, we neglect the sixth post-Newtonian correction in our computations.

While NSs have nonzero tidal deformability, the tidal deformability for BHs is zero. Tidal parameters can be inferred from GW signals, but current measurements have large uncertainties [74,75]. Using GW observations, one can compute the value of $\tilde{\Lambda}$ for the binary system and infer whether the system is a BNS or a BBH [66,76,77].

If the system is a BBH, it could have formed through the imploding DM channel. This allows us to find constraints on DM properties. On the other hand, if none of the systems are concluded to be BBH or NSBH binaries, we can still get limits for the DM properties.

III. TIDAL DEFORMABILITY MEASUREMENT WITH GRAVITATIONAL-WAVE DETECTOR NETWORKS

We now discuss the accuracy with which the effective tidal deformability $\tilde{\Lambda}$ can be measured using the GW signals emitted by coalescing BNSs. We will estimate the accuracy within the Fisher information matrix formalism [78,79], as implemented in GWBENCH [80]. The two ingredients needed for the measurement of $\tilde{\Lambda}$ are (i) a GW detector network, which we introduce in Sec. III A, and (ii) the waveform model used in the Fisher matrix, which we discuss briefly in Sec. III B. Section III C describes the accuracy with which $\tilde{\Lambda}$ can be measured with the detector networks considered in this study.

A. Detector networks

Several authors have studied the capabilities of Advanced LIGO and Advanced Virgo in measuring the tidal deformability of NSs: for a review, see, e.g., [61]. During the second observing run, LIGO and Virgo observed the first BNS inspiral event with a joint SNR of 33 [81] which allowed the measurement of $\tilde{\Lambda}$ to within an accuracy of $\sigma_{\tilde{\Lambda}} = 630$ at 90% credible interval [82], with some authors ruling out the possibility that this was a BBH [74], especially when combined with optical and infrared observations [83]. The second BNS merger event, GW190425, was observed with a far lower SNR of 12.9, and it did not allow placement of any meaningful bounds on the tidal deformability of NSs [84]. The upcoming year-long fourth observing run of the LIGO, Virgo, and KAGRA detectors is expected to detect a handful of BNS mergers, but at the current sensitivity this network will not measure $\tilde{\Lambda}$ with an accuracy good enough to conclusively say that tidal effects are absent. We will therefore restrict ourselves to future upgrades of LIGO, Virgo, KAGRA, and LIGO-Aundh,[1] as well as XG observatories such as Cosmic Explorer [85] and the Einstein Telescope [86].

More precisely, we consider three ground-based detector networks—A+, Voyager, and XG—to determine the accuracy of measuring the effective tidal deformability, with particular interest in the XG network, since these observatories will have the required sensitivities to obtain an informative estimate of the tidal deformability parameter for BNSs.

(i) The A+ network comprises five detectors: LIGO-Hanford, LIGO-Livingston, Virgo, KAGRA, and LIGO-Aundh at A+ sensitivity [87].

(ii) The Voyager network consists of LIGO-Hanford, LIGO-Livingston, and LIGO-Aundh at Voyager sensitivity [88], with Virgo and KAGRA at A+ sensitivities.

(iii) Finally, the XG network includes the Einstein Telescope, one Cosmic Explorer in the U.S., and another Cosmic Explorer in Australia, as in [80].

B. Binary NS waveform model

As discussed in Sec. II, the signature of tidal deformation is imprinted in the GWs emitted by an inspiraling BNS system. The simplest modification of the point-particle post-Newtonian model in the frequency domain—cf. Eq. (4)—captures the essence of the tidal effects, but it is not in agreement with waveforms obtained from numerical simulations of BNS mergers. We adopt the IMRPhenomD_NRTidalv2 waveform model, in which the Fourier amplitude and phase are given algebraically in closed form [89–91]. This choice

---

[1]LIGO-Aundh is the preferred name for the new LIGO-India observatory, coming up near the town of Aundh in central India.

improves the accuracy in the calculation of derivatives of the waveform with respect to the various parameters, which are needed to compute the Fisher matrix.

The tidal terms in this model are valid at frequencies as low as ∼50–100 Hz where Cosmic Explorer and Einstein Telescope have good sensitivity. The model does not incorporate the postmerger signal that could be present if the remnant is a long-lived NS, nor dynamical tides, which could also be important [92–101], although subdominant compared to the static tides that are included in the model.

The waveform model is described by ten parameters (see Table I): the companion masses (m_1, m_2), two angles describing the position of the source in the sky (α, δ), two angles describing the inclination of the binary's orbit and the wave polarization (ι, ψ), the luminosity distance of the source D_L (or, equivalently, its redshift z), the effective tidal parameter $\tilde{\Lambda}$, the coalescence time t_C, and the coalescence phase ϕ_C.

In the Fisher matrix approximation, which involves derivatives with respect to the parameters of the waveform, the absolute error in the measurement of $\tilde{\Lambda}$ at leading post-Newtonian order is the same for all values of $\tilde{\Lambda}$. This is because the effective tidal parameter appears linearly in the waveform model and we have neglected the subdominant tidal terms. Thus, the error $\sigma_{\tilde{\Lambda}}$ is determined by the correlation of $\tilde{\Lambda}$ with the other waveform parameters and the loudness of the signal and not any particular value of $\tilde{\Lambda}$. To compute the Fisher matrix, without loss of generality we use a tidal deformability of $\Lambda_{1,2} = 2$, because a nonzero tidal deformability value is required to use IMRPhenomD_NRTidalv2.

The NS mass distribution is not known very well, but accurate measurement of NSs in radio binary pulsars seems to suggest that they are normally distributed with a standard

TABLE I. Parameter space of BBHs used in this study. In addition to the detector-frame companion masses and the tidal deformability of NSs, there are four angles [two describing the orientation of the binary's orbit relative to the detector frame (ι, ψ) and two for the sky position of the source (α, δ)], the luminosity distance (or, equivalently, redshift z), a fiducial "arrival time" t_C when the strain amplitude of the signal is largest, and the phase of the signal at that time ϕ_C.

Component mass, m_1 and m_2	$[1, 2] M_\odot$
Tidal parameters[a], Λ_1 and Λ_2	2.0
Effective tidal parameter, $\tilde{\Lambda}$	$(6q^2 + q + 6)\Lambda_1/(13q)$
Right ascension, α	$[0, 2\pi)$
Declination, δ	$[-\pi/2, \pi/2]$
Inclination, ι	$[0, \pi]$
Polarization, ψ	$[0, 2\pi]$
Redshift, z	$[0, 10]$
Fiducial time of arrival, t_C	0
Constant phase offset, ϕ_C	0

[a]These parameters do not directly enter the waveform, but only the effective tidal deformability $\tilde{\Lambda}$.

deviation that is small compared to the mean (see [102,103]). The two BNS mergers discovered by LIGO and Virgo, in particular GW190425 [84], already indicate that NS masses in merging binaries could be different from those of Galactic BNSs. There is currently no concrete distribution that we could use from GW measurements (see, however, [104]) and hence we draw the companion masses with a mean value of $1.3M_\odot$ and a standard deviation of $0.09M_\odot$ [103], but with the constraint that $1 \le m_1, m_2 \le 2M_\odot$.

If $\Lambda_1 = \Lambda_2 = \Lambda$, then Eq. (8a) leads to

$$\tilde{\Lambda} = \frac{6q^2 + q + 6}{13q}\Lambda.$$

This implies that for $0.5 \le q \le 1$, which is the range of $q = m_2/m_1$ allowed by the hard upper and lower cutoff of NS masses, $2 \le \tilde{\Lambda} \lesssim 2.5$. The range of $\tilde{\Lambda}$ is a proxy for the mass ratio in our sample, and the variation in the measurement error in $\tilde{\Lambda}$ is determined largely by its correlation with other parameters and by the SNR.

C. Measurement accuracy of $\tilde{\Lambda}$

Bayesian inference is the preferred method to estimate the error in the measurement of parameters, but the long Markov chains needed for the convergence of the posterior distribution are expensive and time consuming. For the exploratory work carried out in this paper, it suffices to employ the faster Fisher matrix approach. In this approach, one first computes the Fisher information matrix Γ_{mn} defined by

$$\Gamma_{mn} \equiv \langle \partial_m \tilde{h}, \partial_n \tilde{h} \rangle, \qquad (9)$$

where ∂_m denotes the derivative of the waveform with respect to the parameter λ_m of the waveform, $\tilde{h}(f)$ is the Fourier transform of the detector response $h(t) \equiv F_+ h_+ + F_\times h_\times$, $(h_+, h_\times)$ are the two polarization strain

amplitudes, and $\langle a, b \rangle$ is the scalar product of waveforms a and b, defined as

$$\langle a, b \rangle \equiv 4\Re \int_{f_L}^{f_H} a(f)b^*(f)\frac{df}{S_h(f)}. \qquad (10)$$

Here $S_h(f)$ is the noise power spectral density of the detector in question, and f_L and f_H are suitably chosen lower and upper frequency cutoffs. We choose $f_L = 20$ Hz for the A+ and Voyager networks and $f_L = 5$ Hz in the case of the XG network. The upper frequency cutoff is chosen to be the Nyquist frequency with a sampling rate of 4096 Hz.

The information matrix of a detector network is just the sum of the individual information matrices: $\Gamma_{mn} \equiv \sum_A \Gamma_{mn}^A$. The covariance matrix is the inverse of Γ: $C_{mn} = (\Gamma^{-1})_{mn}$. By definition the Fisher matrix is symmetric and so is the covariance matrix. Its diagonal elements C_{mm} are the variances in the inference of parameters λ_m, and the off-diagonal elements C_{mn} are the covariances in parameters λ_m and λ_n.

We perform the analysis for a population of BBH sources with component masses $m_1, m_2 \in [1M_\odot, 2M_\odot]$, distributed in redshift as described in Sec. IV, up to a maximum redshift of $z = 10$. Table I lists the parameters of the binary population considered in this study. The errors on the effective tidal deformability $\sigma_{\tilde{\Lambda}}$ for this population were computed using the GWBENCH toolkit [80], which performs Fisher analysis to provide measurement errors on GW parameters given a network of GW detectors. This provides the distribution of inferred values of $\tilde{\Lambda}$ for the cosmic population of sources. We use $\sigma_{\tilde{\Lambda}}^{90\%}$ as the criterion to differentiate between the population of BBHs and BNSs in this mass range because $\tilde{\Lambda} = 0$ for BHs. Therefore, the confidence with which we can classify a binary as a BBH or BNS is inversely proportional to the measurement error, given some $\tilde{\Lambda}$.
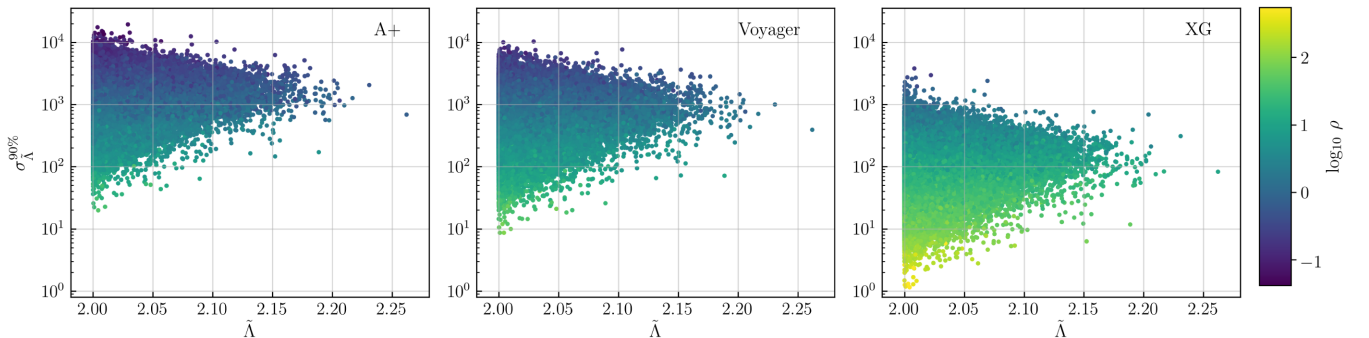

FIG. 3. These plots show $\sigma_{\tilde{\Lambda}}^{90\%}$, the 90% confidence interval in the accuracy of measurement of $\tilde{\Lambda}$, for A+ (left), Voyager (middle), and XG (right), as a function of $\tilde{\Lambda}$ and the SNR (color bar). The measurement accuracy is an order of magnitude better for the XG network compared to the A+ network. In XG detectors, half of all events within $z = 10$ have their tidal deformability constrained to within $\sigma_{\tilde{\Lambda}}^{90\%} \lesssim 100$, an order of magnitude larger for than A+.
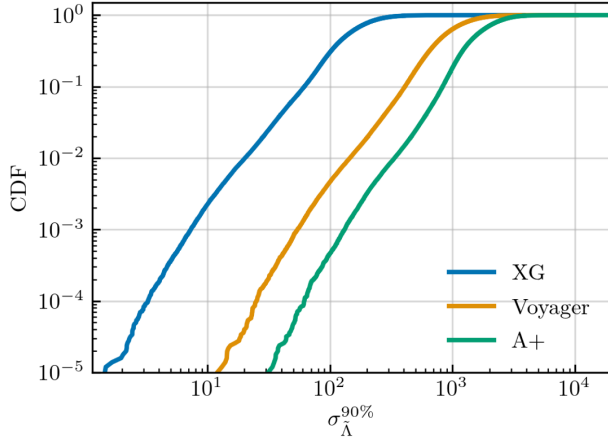
FIG. 4. Cumulative distribution function (CDF) of the error in the measurement of effective tidal deformability in the three detector networks considered in this study. Notice that the fraction of events detected with an error $\sigma_{\tilde{\Lambda}}^{90\%} \simeq 100$ is 0.05%, 0.5%, and 30% in the A+, Voyager, and XG networks, respectively.

The 90% confidence interval in the measurement of the effective tidal deformability for the full population $\sigma_{\tilde{\Lambda}}^{90\%}$ is shown in Fig. 3 for the three networks considered in this study, with the color representing the SNR of the events. In Fig. 4 we plot the cumulative distribution of $\sigma_{\tilde{\Lambda}}^{90\%}$ for the three networks. The A+ and Voyager networks can determine the tidal deformability to within $\sigma_{\tilde{\Lambda}}^{90\%} \simeq 100$ for 0.05% and 0.5% of the population. The XG network, on the other hand, can determine $\tilde{\Lambda}$ to the same accuracy for 30% of the full population. This is a good enough accuracy to distinguish BNSs from BBHs if the preferred EOS is stiff, such as ALF2, producing larger NS radii and greater tidal deformabilities (e.g., $\tilde{\Lambda} \sim 300$ for a $1.4M_\odot$ NS, which is true for most NS masses considered in our study). Smaller errors $\sigma_{\tilde{\Lambda}}^{90\%} \lesssim 20$ would be required if NSs are described by a softer EOS, such as APR4, with tidal deformabilities $\tilde{\Lambda} \sim 50$. A greater measurement accuracy (i.e., smaller values of $\sigma_{\tilde{\Lambda}}^{90\%}$) requires louder signals, which means fewer systems can be classified as belonging to one of the two classes. For example, only the XG network can measure $\tilde{\Lambda}$ to better than $\sigma_{\tilde{\Lambda}}^{90\%} < 20$. Thus, the measurement accuracy of effective tidal deformability directly impacts how well we can determine the collapse time discussed in Sec. V.

IV. MERGER RATES

In this section we discuss how to deduce constraints on DM mass and interaction cross section based on the observed merger rate of BNS and BBH systems in the NS mass range. The constraints follow by comparing the timescale for conversion of NSs to BHs by DM accumulation t_c to the timescale for coalescence of NSs by gravitational radiation

backreaction t_d. The timescales in the problem suggest that either both or neither of the NSs in a binary will be converted to BHs before they inspiral and merge, so we will not consider NSBH binaries, but we will derive an equation that relates an upper limit on the merger rate of BBHs to the properties of DM particles.

A. Collapse timescales and merger time delays

As we shall discuss in Sec. VI, the timescale t_c for NSs to implode to form BHs largely depends on the properties of the DM particles: (i) the interaction cross section σ_χ, (ii) the DM density at the site of BNSs and their dispersion velocity (which are both determined by the location of the binary within a galaxy, being larger at the galactic core and smaller in the halo), and (iii) the mass of the DM particles m_χ. On the other hand, the timescale t_d for NSs to coalesce depends on (i) the eccentricity and semimajor axis when the BNS first forms, and (ii) the masses of the two NSs [69].

The two NSs in a binary do not form from their stellar progenitors at the same time. The delay in the formation of the second NS with respect to the first could be substantial if the masses of the parent stars are very different. However, the timescale arguments in Sec. I imply that binaries with component masses $1M_\odot \leq m \leq 2M_\odot$ will either be BNS or BBH binaries, and not mixed (NSBH) binaries, so we will ignore mixed binaries from now on.

B. Binary neutron star merger rate

LIGO and Virgo have so far observed two BNS mergers: GW170817 at a distance of 40^{+8}_{-14} Mpc [81] and GW190425 at a distance of 159^{+69}_{-72} Mpc [84], both at 90% credible interval (CI). Since they are both at very low redshift, the merger rate determined from them is essentially the local (i.e., $z = 0$) rate. The local rate for BNSs inferred from the third Gravitational-Wave Transient Catalog [6] is $R_0 = 660^{+1040}_{-530}$ Gpc^{-3} yr^{-1} at 90% CI [105], under the assumption of a multisource model including BNS, NSBH, and BBH subpopulations.

The merger rate evolves with redshift because (i) the star formation rate varies as a function of redshift; (ii) BNSs that form at a certain redshift do not merge immediately, but only after a delay time t_d, and hence at a different redshift; and (iii) the metallicity evolves with redshift, affecting the mass function and formation rate of compact binaries. In this study, we will ignore the effect of metallicity, as it plays a greater role in the case of BBHs and is less likely to affect the merger rate of BNSs [34,106–108]. We will assume the star formation rate $\psi(z)$ (SFR) given by Ref. [109],

$$\psi(z|\alpha_F, \beta_F, C_F) \propto \frac{(1+z)^{\alpha_F}}{1 + \left(\frac{1+z}{C_F}\right)^{\beta_F}}, \qquad (11)$$

with $(\alpha_F, \beta_F, C_F) = (2.7, 5.6, 2.9)$. We assume that the merger rate is the same as the SFR except that binaries

that form at redshift z_f merge at redshift z after a delay t_d, with a corresponding redshift interval $\Delta z = z_f - z$. Given a redshift z at which merger rate is required and the time delay t_d, the redshift z_f at which the binary forms can be found by solving

$$t_d = \frac{1}{H_0} \int_z^{z_f} \frac{dz'}{(1+z')E(z')}, \qquad E(z) = \Omega_\Lambda + \Omega_M (1+z)^3, \tag{12}$$

where Ω_M and Ω_Λ are the DM and dark energy densities, respectively, and we have assumed a flat universe in which dark energy is interpreted as a cosmological constant [110]. Now, the merger rate density $\dot{n}(z)$ as a function of redshift can be computed by integrating the SFR over all delay times, the delay-time probability function $P(t_d)$ serving as a weighting factor,

$$\dot{n}(z) = A \int_{t_d^{\min}}^{t_d^{\max}} \psi(z_f(z, t_d))\mathcal{P}(t_d)dt_d, \tag{13}$$

where z_f is found using Eq. (12). The delay-time distribution is not very well known, and we take it to be the Jeffrey's prior $\mathcal{P}(t_d) \propto t_d^{-1}$ extending over the range $[t_d^{\min}, t_d^{\max}]$, with the normalization

$$\int_{t_d^{\min}}^{t_d^{\max}} P(t_d)dt_d = 1.$$

The constant A in Eq. (13) is chosen such that $\dot{n}(0) = R_0$,
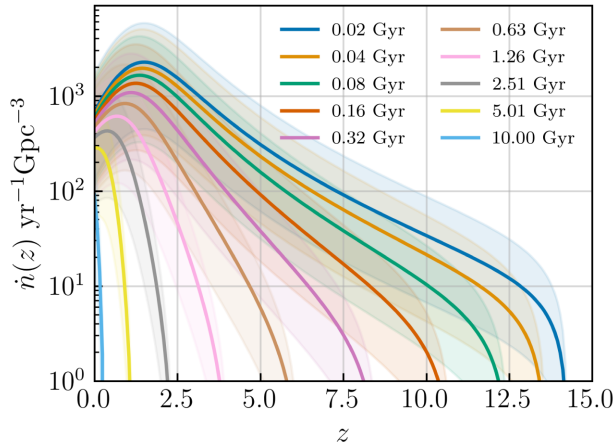
$$A = \frac{R_0}{\int_{t_d^{\min}}^{t_d^{\max}} \psi(z_f(0, t_d))P(t_d)dt_d}. \tag{14}$$

If NSs in a binary implode to form BHs within a collapse time t_c that lies between the minimum and maximum delay times, i.e., $t_d^{\min} < t_c < t_d^{\max}$, then the total merger rate density in Eq. (13) is the sum of the BNS and BBH merger rates, i.e., $\dot{n}_{\text{total}} = \dot{n}_{\text{BNS}} + \dot{n}_{\text{BBH}}$, where

$$\dot{n}(z)_{\text{BNS}} = A \int_{t_d^{\min}}^{t_c} \psi(z_f(z, t_d))\mathcal{P}(t_d)dt_d, \tag{15}$$

$$\dot{n}(z)_{\text{BBH}} = A \int_{t_c}^{t_d^{\max}} \psi(z_f(z, t_d))\mathcal{P}(t_d)dt_d. \tag{16}$$

The left panel of Fig. 5 shows the merger rate of BBHs formed by implosion as a function of redshift for different choices of the collapse time t_c (in gigayears). The shaded region for each choice of t_c represents the uncertainty in the local merger rate of BNS found using the latest GW catalog, which is in the range $130 \leq R_0 \leq 1700$ Gpc^{-3} yr^{-1} [105]. If the collapse time is less than the smallest delay time, then all BNSs are converted to BBHs, and the entire BNS population will be observed as BBHs. If, on the other hand, the collapse time is larger than the largest delay time, no BNS is converted to BBH. The observed population will be a mixture of BNS and BBH for values of the collapse time in between these extremes.

The merger rate $d\dot{N}$ in a cosmological volume dV_c (redshift range dz), as measured by an observer at $z = 0$, is $\dot{N} = \dot{n}(z)dV_c/(1+z)$, where a factor $(1+z)$ accounts for the time dilation between observers at redshift z and
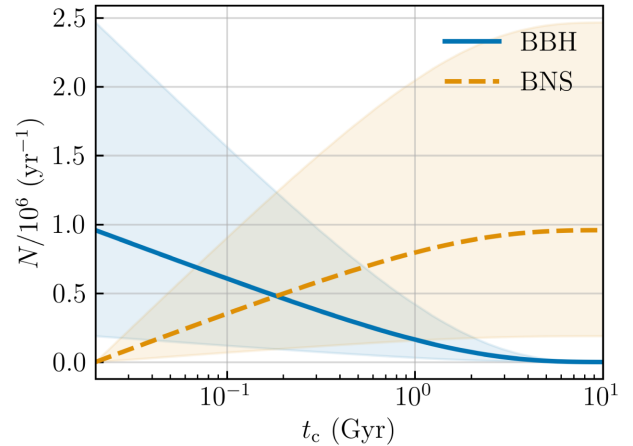

FIG. 5. Left: merger rate density of BBHs formed by implosion as a function of redshift for several values of the collapse time t_c from 0.02 to 10 Gyr, as given in the legend (in gigayears). Right: the number of BNS and BBH mergers per year $N = \dot{N}T$, $T = 1$ yr, in Earth's frame as a function of the collapse time t_c. Not all of these would be observable by a detector network, but only those above a certain SNR threshold. The shaded regions in both panels correspond to the 90% credible interval for the local BNS merger rate for the multisource model in [105].

redshift 0. Thus, the merger rate within some redshift z as measured by an observer at $z = 0$ is given by

$$\dot{N} = \int_0^z \frac{\dot{n}(z')}{1+z'} \frac{dV_c}{dz'} dz'. \quad (17)$$

In our simulations we distribute sources as a function of redshift using the above equation. The right panel of Fig. 5 shows the number of BNS and BBH mergers in the Universe per year $N = \dot{N}T$, with $T = 1$ yr, in Earth's frame, as a function of the collapse time t_c. If $t_c < t_d^{\min}$ every BNS will be converted to a BBH, while $t_c > t_d^{\max}$ would imply none will be converted. At intermediate values of t_c we expect to observe, among all mergers, some that are BBHs.

A detector network only observes those mergers that stand above the detector noise at an acceptably low false alarm rate (say, one false event per year). Thus, the merger rate *observable* by a detector network $\dot{N}_{\mathrm{obs}}$ is

$$\dot{N}_{\mathrm{obs}} = \int_0^z \frac{\dot{n}(z')}{1+z'} \frac{dV_c}{dz'} \epsilon(z') dz'. \quad (18)$$

Here $\epsilon(z)$ is the detection efficiency of a network as a function of redshift, to be discussed below. It measures the fraction of events detected by a given detector network subject to one or more conditions. At the outset, we require an event's SNR to be larger than a preset threshold ρ_T to make a high-confidence detection. For the current network of LIGO/Virgo/KAGRA detectors, a SNR threshold of $\rho_T = 10$ assures that the false alarm rate is no more than a few per year.

In this work we not only wish to make high-confidence detections, but additionally select only those events for which the effective tidal deformability can be measured with a good accuracy—good enough to distinguish BBH mergers (for which $\tilde{\Lambda} = 0$) from BNS mergers (for which

$\tilde{\Lambda} > \tilde{\Lambda}_{\min}^{\mathrm{NS}} \gg 0$). To this end, we require the 90% credible interval $\sigma_{\tilde{\Lambda}}^{90\%}$ in the measurement of $\tilde{\Lambda}$ to be less than a preset threshold $\sigma_{\tilde{\Lambda}_T}$, i.e., $\sigma_{\tilde{\Lambda}}^{90\%} < \sigma_{\tilde{\Lambda}_T}$, and choose the threshold so that it is (significantly) smaller than the smallest value of the effective tidal deformability of BNSs,

$$\sigma_{\tilde{\Lambda}_T} \ll \tilde{\Lambda}_{\min}^{\mathrm{NS}} \equiv \min_{m_1, m_2} \tilde{\Lambda}(m_1, m_2),$$

where m_1 and m_2 are the companion masses. This condition guarantees that a merger is correctly classified as a BNS or a BBH merger with high confidence. Typically, NSs with the largest masses and softest equations of state have the smallest tidal deformability. For equations of state that are still viable, the smallest value of $\tilde{\Lambda}$ varies over the range $\tilde{\Lambda} \in [10, 200]$ [63]. We present our results for several values of the threshold $\sigma_{\tilde{\Lambda}_T}$ restricting the value to be less than 100.

With the conditions on SNR and $\tilde{\Lambda}$ imposed, the efficiency of a detector network is given by

$$\epsilon(z) = \frac{1}{N} \sum_{i=1}^N \Pi\left(\frac{\rho}{\rho_T} - 1 | z\right) \Pi\left(\frac{\sigma_{\tilde{\Lambda}_T}}{\sigma_{\tilde{\Lambda}}} - 1 | z\right), \quad (19)$$

where the sum is over the full population of BNSs and $\Pi(x|z)$ denotes the Heaviside step function: $\Pi(x|z) = 0$ if $x \le 0$, and $\Pi(x|z) = 1$ if $x > 0$ given some redshift z.

The number of BBH mergers observed up to some redshift z in an observing period T is given by

$$N_{\mathrm{BBH}} = \dot{N}_{\mathrm{BBH}} T = T \int_0^z \frac{\dot{n}(z')_{\mathrm{BBH}}}{1+z'} \frac{dV_c}{dz'} \epsilon(z') dz', \quad (20)$$

and similarly for BNSs. Therefore, the number of BBHs we expect to observe in this mass spectrum not only depends on the sensitivity of GW detectors and searches, but also on how well we can measure the tidal effects from these
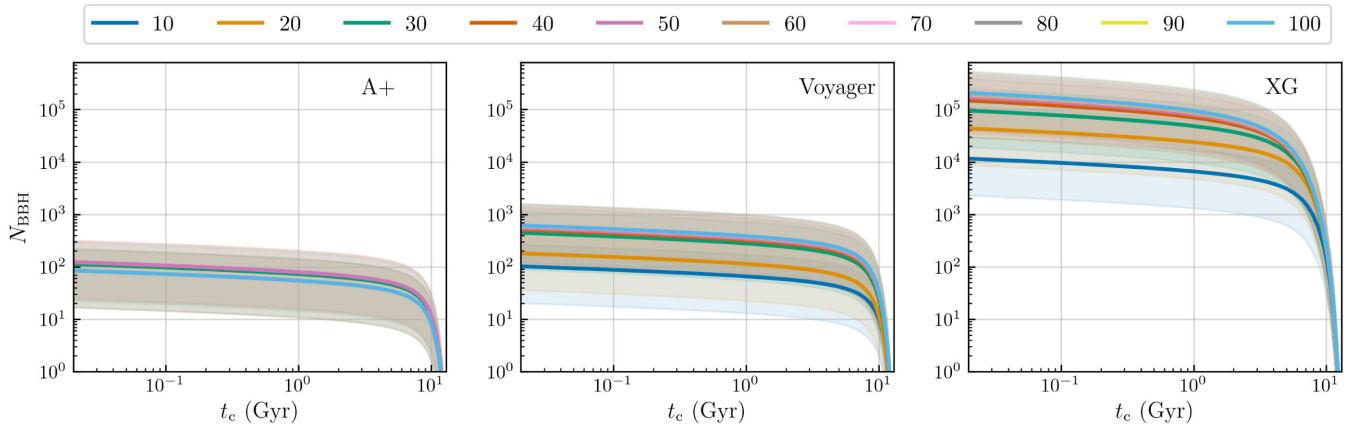

FIG. 6. The number of BBH mergers as a function of collapse time t_c for several values of the threshold $\sigma_{\tilde{\Lambda}_T}$ on the estimated error in $\tilde{\Lambda}$, for five years of observing time.

observations. A single detection with some assumed measurement efficiency for $\tilde{\Lambda}$ provides a limit on t_c which can be used to infer DM properties using Eqs. (33) and (39).

Figure 6 shows the number of BBH mergers observable by a detector network over a five-year duration, $N_{\text{BBH}} = \dot{N}_{\text{BBH}} T$ with $T = 5$ yr, as a function of the collapse time t_c for different choices of the threshold $\sigma_{\tilde{\Lambda}_T}$ (from 10 to 100) and for the A+, Voyager, and XG detector networks described in Sec. III. The imminent upgrade of LIGO and Virgo detectors could identify tens to hundreds of BBHs if the collapse time is in the range of 100 Myr to 1 Gyr over an observational period of five years, but this network is more likely to acquire about a year's worth of data. The Voyager network increases these numbers by an order of magnitude, while the XG network of Einstein Telescope and Cosmic Explorer will observe several orders of magnitude more BH binaries compared to the other networks. As we shall see later, the larger fraction of systems that can be clearly identified as BBH helps in placing tighter constraints on DM mass and interaction cross section.

V. INFERENCE OF COLLAPSE TIME

In this section we elucidate how to infer the average time it takes for a NS to collapse to a BH due to accretion of DM. Let us first note a caveat in our argument: what GWs *can* infer is the relative abundance of BBHs versus BNSs. If BHs with companion masses in the $1 - 2M_\odot$ range form by unknown astrophysical processes or in the primordial Universe, they will be part of the BH population in this mass range and will be indistinguishable from the population that formed from the implosion of NSs due to accumulation of DM. First, we assume that stellar evolution

cannot produce BHs in this mass range. Second, if primordial BHs exist then there is no fundamental reason they should only appear in this mass range. In particular, we expect subsolar mass BBHs to exist as well [111,112]. In the absence of such a population we can be fairly confident (although not certain) that stellar mass BHs in the $1 - 2M_\odot$ range are not of primordial origin. At present, there is no preference for any of these scenarios, so we will proceed with the assumption that any detections of BBHs with BNS masses formed by the implosion of NSs.

Under this assumption, it is straightforward to deduce the collapse time from the observed population of BBHs and BNSs. For illustration, we assume that the true collapse time is $t_c = 1$ Gyr. Given t_c, Eq. (16) gives the local merger rate density, which could then be used in Eq. (20) to compute the number of BBHs expected to be detected over an observational period T in a detector network whose detection efficiency is $\epsilon(z)$, as defined in Eq. (19). Since the rate is Poisson distributed, the number of detections N_{BBH} would be uncertain by $\sqrt{N_{\text{BBH}}}$, and the relative error scales like $1/\sqrt{N_{\text{BBH}}}$.

The left panel of Fig. 7 shows the expected number of BBHs in different detector networks, together with the rate uncertainty in our simulation. The relative uncertainty will, obviously, be larger for less sensitive detectors, and this impacts how well the collapse time can be deduced. The right panel of Fig. 7 shows the collapse time deduced from the rate posterior plotted on the left. In reality, we would determine the number of BBH mergers given the collapse time and network efficiency [i.e., $N_{\text{BBH}}(t_c, \epsilon(z))$] and interpolate this function to determine t_c from N_{BBH} for a given network efficiency $\epsilon(z)$. It is clear that XG detectors will be able to constrain the collapse time far better than the A+ network.
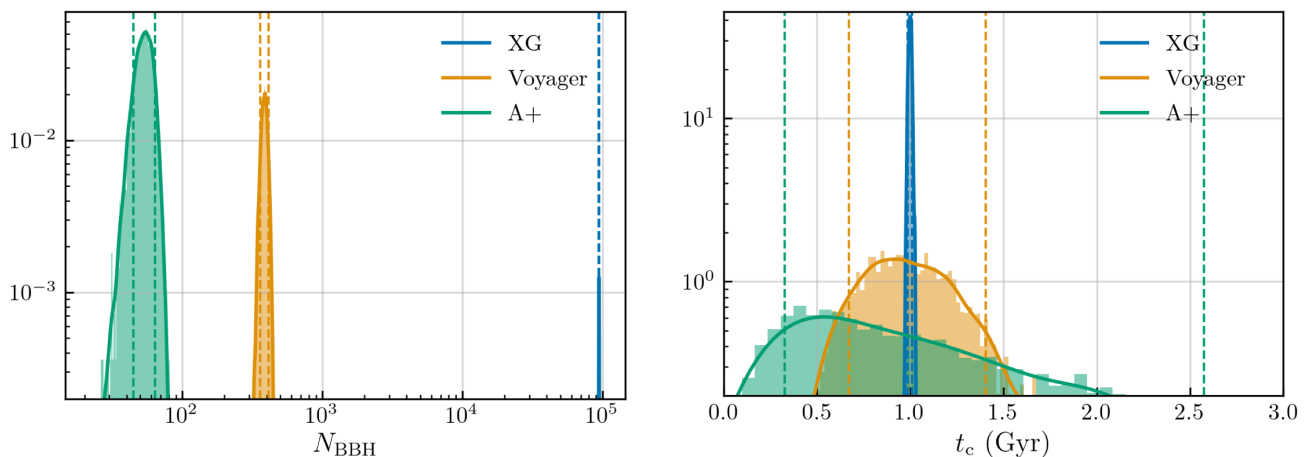

FIG. 7. Left: Gaussian distribution for the observed number of BBHs for $\sigma_{\tilde{\Lambda}_T}^{90\%} = 100$ and $t_c = 1$ Gyr. Right: inferred distribution of t_c from N_{BBH} for the three detector networks under consideration and an observing period of five years. The dashed lines show the 90% credible intervals for the distributions of t_c from N_{BBH}.

VI. IMPLOSION OF NEUTRON STARS BY ACCUMULATION OF DARK MATTER

The inferred collapse time of NSs into BHs from GW observations is model agnostic. These limits can constrain the particle properties of DM in scenarios where DM particles get captured in NS cores. In this section, we illustrate how we can constrain the asymmetric DM scenario under certain simplified assumptions using previously derived limits on the collapse time.

In the asymmetric DM scenario, DM particles do not self-annihilate due to the assumed asymmetry between the number density of particles and antiparticles. Therefore, the capture and accumulation of DM particles in the core of NSs could lead to the formation of a BH at the NS core, leading to the potential implosion of the host star. Here we examine this scenario in the case of noninteracting bosonic DM, because the bosonic Chandrasekhar limit is much lower than that for fermions, implying that bosonic DM undergoes gravitational collapse sooner than fermionic DM. Indeed, the number of fermionic and bosonic particles corresponding to the Chandrasekhar mass for a DM particle of mass m_χ are given, respectively, by

$$N_{\text{Chandra}}^{\text{fermionic}} \simeq 1.8 \times 10^{57} \left(\frac{\text{GeV}}{m_\chi}\right)^3, \qquad (21)$$

$$N_{\text{Chandra}}^{\text{bosonic}} \simeq 1.5 \times 10^{38} \left(\frac{\text{GeV}}{m_\chi}\right)^2. \qquad (22)$$

We also note that, due to the dispersion velocities of DM, the NS gravity alone cannot capture DM particles, and some dissipative mechanism involving the interaction of DM with hadrons would be needed. For the species of DM considered in this paper, DM particles are assumed to interact with hadrons through the weak interaction. However, the accumulation of DM particles over the lifetime of the NS for the accretion rate considered in this paper will not significantly increase its mass.

A. Dark matter capture by neutron stars

The ambient DM attracted by the NS's gravity is captured if its trajectory intersects the star, and it loses energy through its interactions with baryons and leptons. The capture rate of DM by gravitating bodies such as Earth and the Sun was first computed in [113] and a general analytic theory was developed in [114]. These calculations have been refined to include the effects of matter degeneracy in estimating the capture rates of NSs [115,116]. Most recently, the calculations have been further improved to include general relativistic corrections and provide a consistent treatment of several different operator structures that define the interaction between nucleons and DM [117].

The capture rate, in general, depends on the ambient energy density of DM ρ_χ, the DM scattering cross section

off targets in the NSs σ, the number density of targets $n_{\text{t}}(r)$, the escape velocity in the NS at radius r, $v(r)$, the DM velocity dispersion far away from the star v_χ, and the velocity of the NS v_*. In what follows, we adopt the result derived in [117] to obtain the total capture rate for DM in the mass range 1–10^6 GeV and a constant cross section σ.

In this mass range, Pauli blocking suppression of scattering is unimportant, but the momentum transfer involved in DM-nucleon scattering $q \simeq m_\chi v$, where $v = v_{\text{esc}} = \sqrt{2GM_*/R_*} = 0.6c$ is the velocity of the infalling DM, is large. Consequently, corrections due to the finite size of the nucleon included through proper treatment of the nucleon form factors can play a role [118]. Further, the composition of matter and the modification of baryons at high density are also relevant when DM couples to a nucleon property (such as its scalar, pseudoscalar, or axial charge) that can be altered in the dense medium [118,119]. These findings imply that the capture rate will depend on how DM couples to baryons and the composition of the NSs. However, for a given scenario in which the mass of the DM, the form of its coupling to nucleons, and the NS structure and composition have been specified, it is still possible to define an effective cross section σ and write the total capture rate as

$$C_{\text{NS}} = C_{\text{geom}} \text{Min}\left[\frac{\sigma}{\sigma_{\text{th}}}, 1\right], \qquad (23)$$

where

$$C_{\text{geom}} = \pi R_*^2 \frac{\rho_\chi}{m_\chi} v_* \text{Erf}\left[\sqrt{\frac{3}{2}}\frac{v_*}{v_\chi}\right] \frac{(v_{\text{esc}}^2/v_*^2)}{1 - (v_{\text{esc}}^2/c^2)} \qquad (24)$$

is the geometric capture rate that includes the effect of gravitational focusing in general relativity, and

$$\sigma_{\text{th}} = \frac{\pi R_*^2}{N_{\text{t}}\xi} \qquad (25)$$

is the threshold value of the cross section required to ensure that the DM particles traversing the NS have at least one collision. Here, N_{t} is the total number of target particles in the NS, and

$$\xi = \frac{4\pi}{N_{\text{t}}} \int_0^{R_*} r^2 dr \sqrt{g_{rr}(t)} n_{\text{t}}(r) \frac{1 - g_{tt}(r)}{1 - g_{tt}(R_*)} \frac{g_{tt}(R_*)}{g_{tt}(r)}, \qquad (26)$$

where g_{tt} and g_{rr} are temporal and spatial components of the Schwarzschild metric. The dimensionless number $\xi \approx \mathcal{O}(1)$ and its precise value depends on the structure of the NS and the density profile of targets in the NS interior.

For a typical NS with mass $M_* \simeq 1.4 M_\odot$, radius $R_* = 12$ km, and total baryon number $N_t \simeq 2 \times 10^{57}$, assuming that $\xi \approx 1$, the threshold cross section

$\sigma_{\mathrm{th}} \approx 2 \times 10^{-45}$ cm^2. For this case, the accumulation of DM in a NS at rest, i.e., $v_* = 0$, is given by

$$N_\chi(t) = \sqrt{6\pi} R_*^2 \frac{\rho_\chi}{m_\chi} \frac{(v_{\mathrm{esc}}^2/v_\chi)}{1 - (v_{\mathrm{esc}}^2/c^2)} \mathrm{Min}\left[\frac{\sigma}{\sigma_{\mathrm{th}}}, 1\right] t. \quad (27)$$

Using $v_{\mathrm{esc}} = \sqrt{2GM_*/R_*} = 0.6c$, and a DM velocity dispersion $v_\chi = 220$ km/s, we obtain

$$N_\chi(t) = 2.9 \times 10^{43} \frac{\rho_\chi}{\rho_0} \left(\frac{\mathrm{GeV}}{m_\chi}\right) \mathrm{Min}\left[\frac{\sigma}{\sigma_{\mathrm{th}}}, 1\right] \frac{t}{10^{10}\ \mathrm{yr}}, \quad (28)$$

where $\rho_0 = 1$ GeV/cm^3 is our choice for the fiducial DM density.

B. Thermalization and formation of a mini black hole

The captured DM particles continue to scatter and eventually thermalize with NS matter. A general analysis of thermalization is challenging because the DM energy decreases over several orders of magnitude during this process. At low energy, matter degeneracy and correlations due to strong interactions between baryons can substantially alter the scattering rate [120,121]. For scattering off neutrons with a constant cross section, the thermalization time for the DM masses of interest is

$$t_{\mathrm{th}} \simeq 3750\ \mathrm{yr} \frac{\gamma}{(1+\gamma)^2} \left(\frac{2 \times 10^{-45}\ \mathrm{cm}^2}{\sigma_\chi}\right) \left(\frac{10^5\ \mathrm{K}}{\mathrm{T}}\right), \quad (29)$$

where $\gamma = m_\chi/m_{\mathrm{n}}$, and m_{n} is the neutron mass [120].

Upon thermalization, the radius of the DM sphere is determined by the temperature and the gravitational potential of the NS [120]

$$r_{\mathrm{th}} \approx 2.2\ \mathrm{m} \left(\frac{\mathrm{T}}{10^5\ \mathrm{K}}\right)^{1/2} \left(\frac{1\ \mathrm{GeV}}{m_\chi}\right)^{1/2}. \quad (30)$$

When the mass density of bosonic DM exceeds that of baryons, the DM becomes self-gravitating. This occurs when the total number of DM particles exceeds

$$N_{\mathrm{self}} \simeq 4.8 \times 10^{46} \left(\frac{\mathrm{GeV}}{m_\chi}\right)^{5/2} \left(\frac{\mathrm{T}}{10^5\ \mathrm{K}}\right)^{3/2}. \quad (31)$$

The self-gravitating DM sphere collapses to form a BH when its mass exceeds the Chandrasekhar limit for bosonic matter, i.e., if $N_{\mathrm{self}} > N_{\mathrm{Chandra}}^{\mathrm{bosonic}}$. Using Eq. (21), we can deduce that $N_{\mathrm{self}} > N_{\mathrm{Chandra}}^{\mathrm{bosonic}}$ for $m_\chi \lesssim 10^{17}$ GeV(T/10^5 K)^3. Thus, for the mass range $m_\chi \in [1, 10^6]$ GeV considered here, a mini-BH of mass

$$M_{\mathrm{BH}} = m_\chi N_{\mathrm{self}} \simeq 4.8 \times 10^{46} \left(\frac{\mathrm{GeV}}{m_\chi}\right)^{3/2} \left(\frac{\mathrm{T}}{10^5\ \mathrm{K}}\right)^{3/2} \mathrm{GeV} \quad (32)$$

forms at time

$$t_{\mathrm{BH}} = \frac{N_{\mathrm{self}}}{C_{\mathrm{geom}}} \mathrm{Max}\left[\frac{\sigma_{\mathrm{th}}}{\sigma}, 1\right]$$

$$\approx 10^{13} \left(\frac{\rho_0}{\rho_\chi}\right) \left(\frac{\mathrm{GeV}}{m_\chi}\right)^{3/2} \mathrm{Max}\left[\frac{\sigma_{\mathrm{th}}}{\sigma}, 1\right] \mathrm{yr} \quad (33)$$

when $N_\chi(t_{\mathrm{BH}}) = N_{\mathrm{self}}$. For $\rho_\chi \simeq \rho_0$, collapse occurs at $t < 10^{10}$ yr for $m_\chi \gtrsim 100$ GeV.

C. Bose-Einstein condensation

In the preceding discussion, we neglected the formation of a Bose-Einstein condensate of DM. Earlier work has shown that a BEC can accelerate BH formation for bosonic DM with mass $m_\chi < m_{\mathrm{BEC}}$, where $m_{\mathrm{BEC}} \simeq 2 \times 10^4$ GeV for $T = 10^5$ K and $m_{\mathrm{BEC}} \simeq 5 \times 10^3$ GeV for $T = 10^6$ K [115,122]. We briefly summarize their findings below.

When the critical temperature for BEC of DM

$$T_C = \frac{2\pi}{m_\chi} \left(\frac{3N_\chi(t)}{4\pi r_{\mathrm{th}}^3 \zeta(3/2)}\right)^{2/3} \quad (34)$$

exceeds the NS temperature, a condensate forms at the core within a radius

$$r_{\mathrm{BEC}} = 1.5 \times 10^{-4}\ \mathrm{cm} \left(\frac{1\ \mathrm{GeV}}{m_\chi}\right)^{1/2} \quad (35)$$

which is much smaller than r_{th}. This occurs when the total number of accumulated DM,

$$N_\chi(t) = N_{\mathrm{C}} = 10^{36} \left(\frac{T}{10^5\ \mathrm{K}}\right)^3, \quad (36)$$

and the number of DM particles in the condensate,

$$N_{\mathrm{BEC}}(t) = N_\chi(t) - N_\chi(t) \left(\frac{T}{T_C}\right)^{3/2} = N_\chi(t) - N_C, \quad (37)$$

increase at the accretion rate on timescales that are large compared to the thermalization time. The BEC becomes self-gravitating when $N_{\mathrm{BEC}} > 4\pi r_{\mathrm{BEC}}^3 \rho_B/m_\chi \approx 10^{28}(\mathrm{GeV}/m_\chi)$. Since $N_{\mathrm{BEC}} \ll N_{\mathrm{Chandra}}^{\mathrm{bosonic}}$ for the mass range of interest, the self-gravitating BEC is stable, and the time required for it to collapse is obtained as a solution to $N_\chi(t_{\mathrm{BH}}^{\mathrm{BEC}}) = N_{\mathrm{Chandra}}^{\mathrm{bosonic}} + N_C$. We find that a BH of mass

$$M_{\text{BH}}^{\text{BEC}} = m_\chi N_{\text{Chandra}}^{\text{bosonic}} \simeq 1.5 \times 10^{38} \left(\frac{\text{GeV}}{m_\chi} \right) \text{ GeV} \quad (38)$$

forms at a time

$$t_{\text{BH}}^{\text{BEC}} = \frac{N_{\text{Chandra}}^{\text{bosonic}} + N_C}{C_{\text{geom}}} \text{Max} \left[\frac{\sigma_{\text{th}}}{\sigma}, 1 \right]$$

$$\approx 5.2 \times 10^4 \left(\frac{\rho_0}{\rho_\chi} \right) \left(\frac{\text{GeV}}{m_\chi} \right) \text{Max} \left[\frac{\sigma_{\text{th}}}{\sigma}, 1 \right]$$

$$\times \left[1 + \frac{2}{3} \left(\frac{m_\chi}{10 \text{ GeV}} \right)^2 \left(\frac{T}{10^5 \text{ K}} \right)^3 \right] \text{ yr.} \quad (39)$$

At $T = 10^5$ K, this equation implies $t_{\text{BH}}^{\text{BEC}} < t_{\text{BH}}$ for $m_\chi < 2 \times 10^4$ GeV, and BEC greatly reduces the time for BH formation in this mass range. For example, when $m_\chi = 1$ GeV, the BEC reduces the collapse time by $\approx 10^8$ yr. Consequently, mini-BH formation is possible within the Universe's lifetime for the range of DM considered in this study ($m_\chi = 1 - 10^6$ GeV).

D. Growth of the black hole due to accretion of baryons

The mini-BH continues to grow if the Bondi-Hoyle accretion rate, $\dot{M}_{\text{acc}} = 4\pi\lambda_s (GM_{\text{BH}}/v_s^2)^2 \rho_C v_s$, exceeds the Hawking evaporation rate, $\dot{M}_{\text{evap}} = (15360\pi G^2 M_{\text{BH}}^2)^{-1}$, where v_s is the sound speed, ρ_C is the central baryon density of the NS surrounding the BH, M_{BH} is the mass of the BH at the star's core, and λ_s is a dimensionless constant that depends on the EOS of matter in the NS core. The growth is possible only if the BH reaches a critical mass,

$$M_{\text{BH}}^{\text{crit}} \simeq 1.3 \times 10^{37} \left(\frac{v_s}{0.3c} \right)^{3/4} \left(\frac{10^{15} \text{g/cm}^3}{\lambda_s \rho_B} \right)^{1/4} \text{ GeV.} \quad (40)$$

The analysis of BH growth rates presented in Refs. [115,122] use $\lambda_s = 1/4$, corresponding to a polytropic index $\Gamma = 5/3$. Since the EOS of the NS core is expected to be stiff, with $\Gamma \simeq 2$ and $v_s \simeq c/\sqrt{3}$, there has been much recent work on understanding Bondi-Hoyle accretion under these conditions [123–128]. These studies suggest $\lambda_s \simeq 1.3$ for realistic NS equations of state.

For the scenario in which a BH forms without a BEC intermediate state, i.e., for $m_\chi \gtrsim m_{\text{BEC}}$, from Eqs. (32) and (40) we find that $M_{\text{BH}} > M_{\text{BH}}^{\text{crit}}$ for the mass range of interest. In the scenario that involves a BEC intermediate state, i.e., for $m_\chi < m_{\text{BEC}}$, comparing Eqs. (38) and (40) we find that $M_{\text{BH}} > M_{\text{BH}}^{\text{crit}}$ is only satisfied for $m_\chi \lesssim 10$ GeV. For larger m_χ the BH evaporates, because the accretion of baryons cannot keep pace with mass loss from Hawking radiation.

E. Growth due to dark matter accretion

If the thermalization time is short compared to the BH Hawking evaporation time $t_{\text{Haw}} = 15360\pi G^2 M_{\text{BH}}^3/3 \simeq 5 \times 10^4$ yr$(100 \text{ GeV}/m_\chi)^3$, DM accreting onto the NS reaches the BEC efficiently. The maximal impact parameter for DM capture is larger than the radius of the BEC, and DM particles reaching the BEC can feed the growth of the BH at a rate $\dot{M}_{\text{DM}} = C_{\text{NS}}t$ if Hawking radiation does not disrupt the BEC [115]. Direct heating of DM will be absent if the dark sector does not contain mediator particles with mass less than the Hawking temperature $T_{\text{Haw}} = 1/(8\pi GM_{\text{BH}})$. Further, even when DM is directly heated by Hawking radiation, the change in its temperature would be negligible if it can thermalize with baryons quickly [115]. In this case, $\dot{M}_{\text{DM}} = C_{\text{NS}}t > \dot{M}_{\text{evap}}$, and the accretion of DM prevents BH evaporation for heavier masses [115]. Comparing the timescales for thermalization and evaporation, we find that DM accretion can prevent BH evaporation for $m_\chi \lesssim 4 \times 10^3 (\sigma_\chi/\sigma_{\text{th}})(T/10^5 \text{ K})$ GeV.

F. Neutron star implosion timescale

The timescale for a mini-BH to devour the entire NS by Bondi-Hoyle accretion has been computed recently for the stiff EOS expected in NS cores [124]. For a realistic NS model, they estimate this timescale to be given by

$$t_{\text{dev}} \simeq 0.3 \left(\frac{10^{46} \text{ GeV}}{M_{\text{BH}}} \right) \text{ yr,} \quad (41)$$

where M_{BH} is the mass of the initial mini-BH. For large DM mass, i.e., $m_\chi > m_{\text{BEC}}$ where $m_{\text{BEC}} \simeq 2 \times 10^4$ GeV at $T = 10^5$ K, the NS is destroyed on a timescale $t \approx 6 \times 10^{-2} (m_\chi/\text{GeV})^{3/2} (10^5 \text{ K}/T)^{3/2}$ yr. For $m_\chi < m_{\text{BEC}}$ (which involves a BEC intermediate state), the NS is destroyed on a timescale $t \approx 3.2 \times 10^7 (m_\chi/\text{GeV})$ yr.

VII. CONSTRAINING DARK MATTER PROPERTIES FROM THE IMPLOSION TIMESCALE

As discussed before, GW observations can determine the relative abundance of BBHs and BNSs, which allows us to infer the implosion timescale t_c. The posterior distribution of t_c, or the lower bound on t_c if GW observations cannot conclusively measure a nonzero BBH rate, can be used to constrain a region in the space of DM mass, interaction cross section, and dispersion velocity in the vicinity of merger. To illustrate the sensitivity of this method, we assume that the time it takes for DM particle capture to form a BH of critical mass $M_{\text{BH}}^{\text{crit}}$ is approximately equal to the total collapse time t_c of the NS to form a BH through this channel. Furthermore, for illustration, we assume that $t_c = 1$ Gyr.
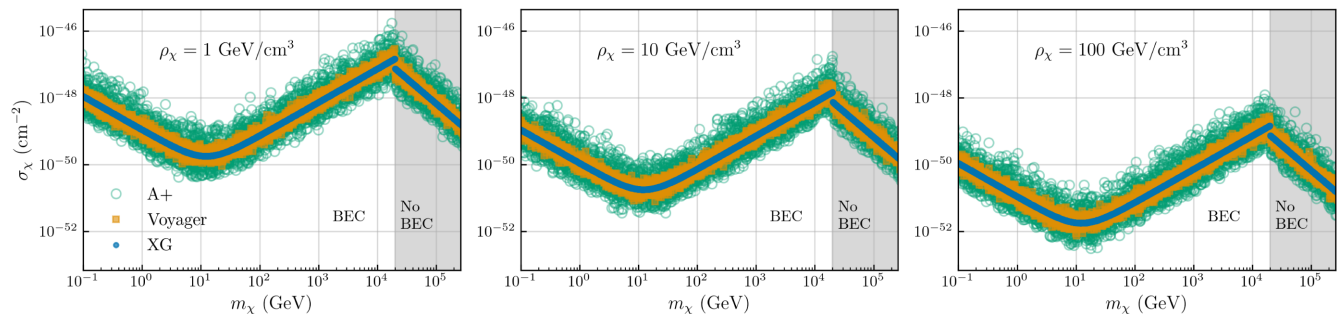
FIG. 8.   Distribution for the mass $m_\chi \in [10^{-1}, 2.5 \times 10^5]$ GeV and scattering cross section σ_χ inferred from the collapse time derived from the observed number of BBHs by the detector networks considered in Fig. 7. Here we consider the scenario where the NS implodes without the formation of a BEC state for $m_\chi \geq 2 \times 10^4$ GeV, shown in gray. For $m_\chi < 2 \times 10^4$ GeV, NS implosion occurs at shorter timescales through the formation of a BEC. We use $\rho_\chi = [1, 10, 100]$ GeV/cm^3.

Figure 8 shows the constraint on the DM particle mass m_χ and the DM-baryon interaction cross section σ_χ for the inferred collapse times shown in Fig. 7 and three values of the DM density: $\rho_\chi = 1$, 10, and 100 GeV/m^3. In all cases, the dispersion velocity is assumed to be 200 km/s. As discussed earlier in Sec. VI A, the limits on the effective cross section shown in Fig. 8 can be used to constrain specific DM scenarios in which the nature of the DM coupling to baryons is defined. Corrections due to the baryon form factors and the modification of baryonic properties at high density need to be accounted for in deriving the limits on the DM-baryon cross section. For the heaviest DM considered in this work, the suppression of the scattering cross section due to the form factors can be quite significant, resulting in bounds that are 2–3 orders of magnitude weaker [118]. However, such a detailed analysis, which is beyond the scope of this work, will also depend on the composition and distribution of baryons in the NS [119]. The precision of the inference of DM

parameters is directly related to how precisely we can deduce the collapse time from the observed number of BBH mergers and the measured $\tilde{\Lambda}$ from the GW signal. Compared to the A+ network, the XG network of Cosmic Explorer and Einstein Telescope can improve the width of the distribution by almost a factor of 10. From Fig. 9, these constraints are competitive with those of direct detection DM experiments, such as the LUX-ZEPLIN (LZ) experiment [129], over the entire range of m_χ. Note, however, that constraints placed by the LZ experiment in this mass range are insensitive to corrections due to the nucleon form factors, since the momentum transfer is small for DM scattering in terrestrial experiments. The effect of variations in the true collapse time on the inferred bounds is discussed in the Appendix.

VIII. CONCLUSIONS AND FUTURE PROSPECTS

In the last decade, direct detection experiments for DM have proven to be successful in constraining the parameter space for weakly interacting massive particles (WIMPs) as well as axionic DM [129–133]. Microlensing surveys [134,135] and calculations from dwarf-galaxy dynamics [136,137], as well as searches for subsolar mass compact binary mergers in GW data [10,11,112,138] have probed the DM compact object parameter space, deriving limits on the abundance of DM in these objects and on their mass spectrum.

In this work, we present a method to combine measurements from GW observations with the particle properties of DM, especially in the WIMP mass range, through the observation (or lack thereof) of a novel population of BBHs in the mass range $1M_\odot \leq m \leq 2M_\odot$. With XG ground-based GW detectors, our ability to measure the effective tidal deformability will improve tremendously, as shown in Fig. 4. With this refinement, we expect to identify a significant number of BBH mergers in this mass range, if this population exists in the Universe. The observed number of mergers can potentially constrain the implosion time of NSs if these BHs form from the collapse of old NSs
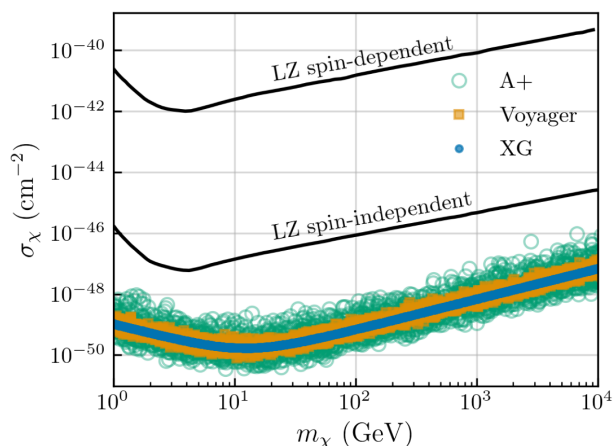

FIG. 9.   Comparison between the constraints obtained for $m_\chi \in [1, 10^4]$ GeV with the lowest ambient DM density considered in this work ($\rho_\chi = 1$ Gev/cm^3) with the latest constraints from the direct detection experiment, LZ [129].

due to the presence of a mini-BH at their cores. If the mini-BH forms through the accumulation of DM in the cores of NSs over their lifetime, the collapse time can then inform us on DM particle properties.

We illustrate how this mechanism works. We report limits on the effective DM-baryon cross section defined by Eq. (23) in a scenario where asymmetric DM is captured through scattering within NS cores to form a self-gravitating mass that collapses to produce a BH. As expected, the constraints are more precise in the case of XG GW detectors, which is a direct consequence of how precisely the binary's effective tidal deformability, and hence the collapse time, is inferred from the observed number of BBH mergers.

One potential issue is the degeneracy with primordial BHs, which could also populate this spectrum of masses. One possible way to remove the degeneracy involves accurate spin measurements to distinguish between the two formation channels. Furthermore, if primordial BHs contribute to the supersolar mass range, we would also expect to observe some subsolar mass primordial BHs. The absence of observed old NSs also complements the observation of BHs formed from imploding NSs. In this work, we show how effectively GW detections can not only constrain DM interactions, but also rule out models that allow for NSs to implode through DM accumulation if no such population is observed in the future.

Multimessenger measurements could help distinguish BBH from BNS mergers. However, Rubin will observe BNS mergers only up to a redshift of $z = 0.3$, while XG detectors will have much deeper reach, extending beyond $z = 2$ (see, e.g., [80], Fig. 2), implying that only ~1% of all BNS mergers detectable in GWs will have EM counterparts. As we have shown in Fig. 3, XG detectors can measure the tidal deformability parameter with high fidelity for most of the sources they observe. Consequently,

including multimessenger observations will only marginally improve the limits on DM properties.

APPENDIX: EFFECT OF COLLAPSE TIME AND DARK MATTER DENSITY ON THE DERIVED LIMITS

In Secs. V and VII, as an illustration of the method, we have assumed $t_c = 1$ Gyr to derive the distribution of merger rates and the resulting constraints on the DM scattering cross section σ_χ and mass m_χ. Here, we discuss
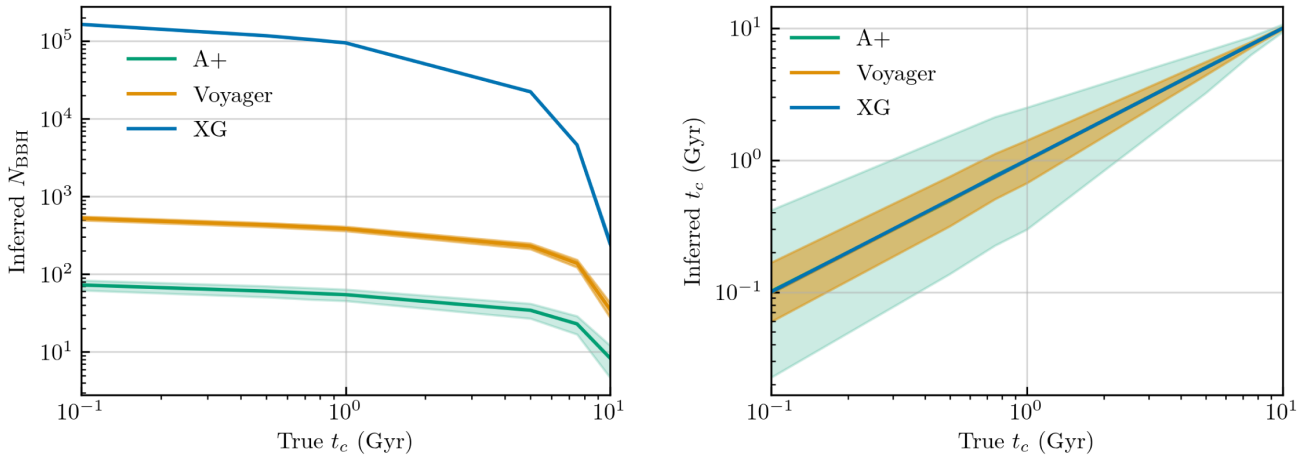

FIG. 10.   Left: median N_{BBH} for $\sigma_{\tilde{\Lambda}_T}^{90\%} = 100$ and for range of values of the true collapse time t_c. Right: inferred median of t_c from the N_{BBH} distributions for the three detector networks under consideration and for an observing period of five years. The colored bands correspond to the 90% credible intervals for the distributions of t_c and N_{BBH}.
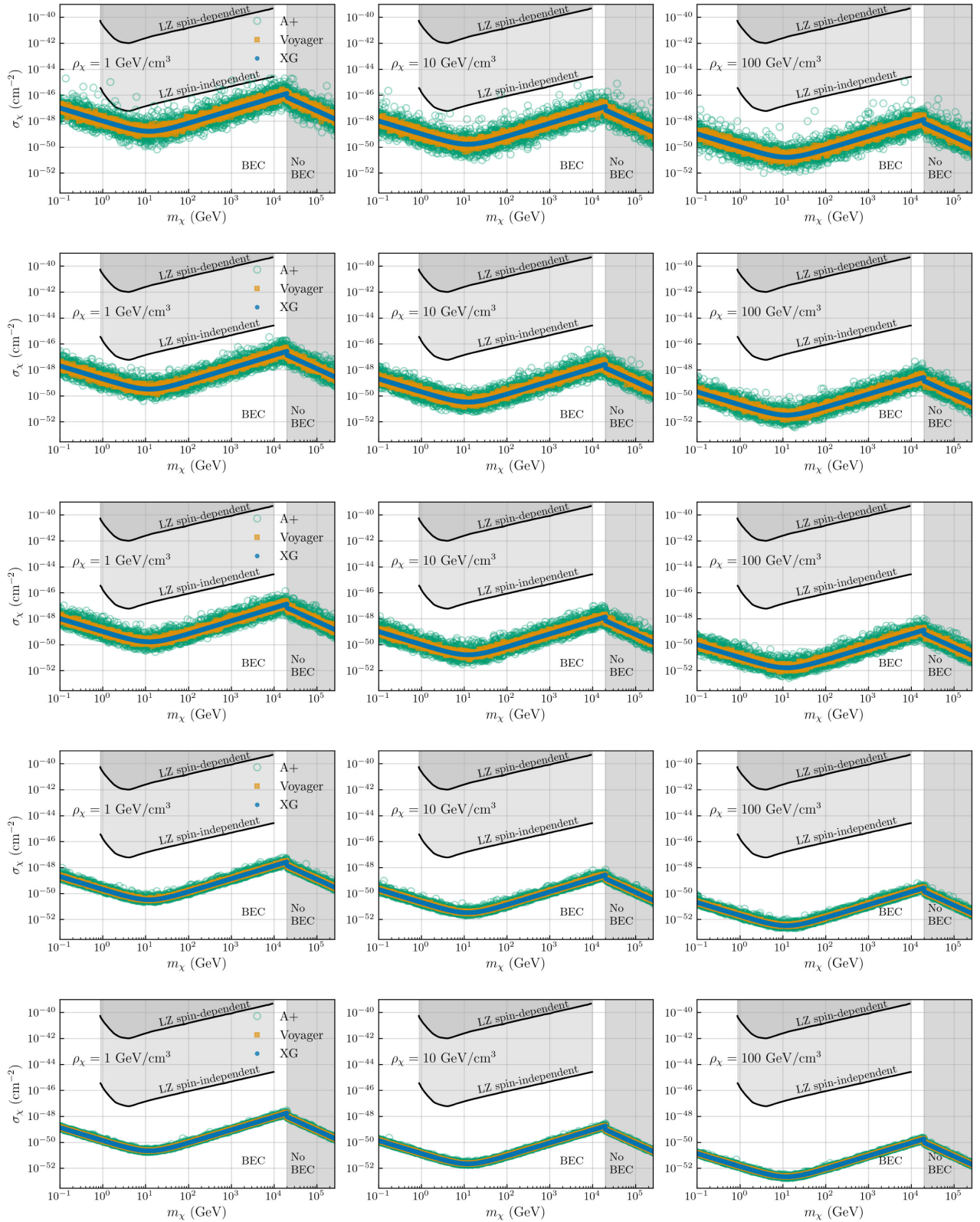
FIG. 11. Distribution of the mass $m_\chi \in [10^{-1}, 2.5 \times 10^5]$ GeV and scattering cross section σ_χ for benchmark values of $\rho_\chi = [1, 10, 100]$ GeV/cm^3 (left to right) and $t_c = [0.1, 0.5, 1, 5, 7.5]$ Gyr (top to bottom).

the effect of varying the collapse time and the DM density ρ_χ.

In Fig. 10 (left panel) we show that, as the collapse time increases, the number of observed BBH mergers decreases (as expected) for all detector networks. The right panel shows that the errors in the inferred collapse time are much higher for A+ due to the lower number of expected observable events. For the XG network, the collapse time is inferred most accurately (as expected).

In Fig. 11 we show how the derived limits on the mass and scattering cross section of the DM particles vary as we change ρ_χ and the true collapse time t_c. The constraints on σ_χ become more stringent as t_c and ρ_χ increase. In addition, the dispersion in the limits derived for A+ and Voyager reduces as t_c increases. This is because when t_c is large, the number of expected observable mergers is closer to the total merger rate, and the merger rate densities peak at small redshifts.

[1] D. J. E. Marsh and S. Hoof, arXiv:2106.08797.

[2] G. Bertone, D. Hooper, and J. Silk, Phys. Rep. **405**, 279 (2005).

[3] B. Carr and F. Kuhnel, Annu. Rev. Nucl. Part. Sci. **70**, 355 (2020).

[4] B. P. Abbott *et al.* (LIGO Scientific and Virgo Collaborations), Phys. Rev. X **9**, 031040 (2019).

[5] R. Abbott *et al.* (LIGO Scientific and Virgo Collaborations), Phys. Rev. X **11**, 021053 (2021).

[6] R. Abbott *et al.* (LIGO Scientific, VIRGO, and KAGRA Collaborations), arXiv:2111.03606.

[7] S. Bird, I. Cholis, J. B. Muñoz, Y. Ali-Haïmoud, M. Kamionkowski, E. D. Kovetz, A. Raccanelli, and A. G. Riess, Phys. Rev. Lett. **116**, 201301 (2016).

[8] K. W. K. Wong, G. Franciolini, V. De Luca, V. Baibhav, E. Berti, P. Pani, and A. Riotto, Phys. Rev. D **103**, 023026 (2021).

[9] G. Franciolini, V. Baibhav, V. De Luca, K. K. Y. Ng, K. W. K. Wong, E. Berti, P. Pani, A. Riotto, and S. Vitale, Phys. Rev. D **105**, 083526 (2022).

[10] B. P. Abbott *et al.* (LIGO Scientific and Virgo Collaborations), Phys. Rev. Lett. **121**, 231103 (2018).

[11] B. P. Abbott *et al.* (LIGO Scientific and Virgo Collaborations), Phys. Rev. Lett. **123**, 161102 (2019).

[12] K. K. Y. Ng, G. Franciolini, E. Berti, P. Pani, A. Riotto, and S. Vitale, Astrophys. J. Lett. **933**, L41 (2022).

[13] V. De Luca, G. Franciolini, P. Pani, and A. Riotto, J. Cosmol. Astropart. Phys. 11 (2021) 039.

[14] K. Eda, Y. Itoh, S. Kuroyanagi, and J. Silk, Phys. Rev. Lett. **110**, 221101 (2013).

[15] K. Eda, Y. Itoh, S. Kuroyanagi, and J. Silk, Phys. Rev. D **91**, 044045 (2015).

[16] O. A. Hannuksela, K. W. K. Wong, R. Brito, E. Berti, and T. G. F. Li, Nat. Astron. **3**, 447 (2019).

[17] O. A. Hannuksela, K. C. Y. Ng, and T. G. F. Li, Phys. Rev. D **102**, 103022 (2020).

[18] B. J. Kavanagh, D. A. Nichols, G. Bertone, and D. Gaggero, Phys. Rev. D **102**, 083006 (2020).

[19] L. Annulli, V. Cardoso, and R. Vicente, Phys. Rev. D **102**, 063022 (2020).

[20] D. Traykova, K. Clough, T. Helfer, E. Berti, P. G. Ferreira, and L. Hui, Phys. Rev. D **104**, 103014 (2021).

[21] A. Coogan, G. Bertone, D. Gaggero, B. J. Kavanagh, and D. A. Nichols, Phys. Rev. D **105**, 043009 (2022).

[22] R. Vicente and V. Cardoso, Phys. Rev. D **105**, 083008 (2022).

[23] N. Speeney, A. Antonelli, V. Baibhav, and E. Berti, Phys. Rev. D **106**, 044027 (2022).

[24] P. S. Cole, A. Coogan, B. J. Kavanagh, and G. Bertone, arXiv:2207.07576.

[25] A. Arvanitaki and S. Dubovsky, Phys. Rev. D **83**, 044026 (2011).

[26] R. Brito, V. Cardoso, and P. Pani, Lect. Notes Phys. **906**, 1 (2015).

[27] A. Arvanitaki, M. Baryakhtar, and X. Huang, Phys. Rev. D **91**, 084011 (2015).

[28] R. Brito, S. Ghosh, E. Barausse, E. Berti, V. Cardoso, I. Dvorkin, A. Klein, and P. Pani, Phys. Rev. Lett. **119**, 131101 (2017).

[29] R. Brito, S. Ghosh, E. Barausse, E. Berti, V. Cardoso, I. Dvorkin, A. Klein, and P. Pani, Phys. Rev. D **96**, 064050 (2017).

[30] K. K. Y. Ng, S. Vitale, O. A. Hannuksela, and T. G. F. Li, Phys. Rev. Lett. **126**, 151102 (2021).

[31] S. Ghosh, E. Berti, R. Brito, and M. Richartz, Phys. Rev. D **99**, 104030 (2019).

[32] C. Yuan, R. Brito, and V. Cardoso, Phys. Rev. D **104**, 044011 (2021).

[33] J. Bramante and T. Linden, Phys. Rev. Lett. **113**, 191301 (2014).

[34] M. Dominik, K. Belczynski, C. Fryer, D. Holz, E. Berti, T. Bulik, I. Mandel, and R. O'Shaughnessy, Astrophys. J. **759**, 52 (2012).

[35] M. Safarzadeh and E. Berger, Astrophys. J. Lett. **878**, L12 (2019).

[36] M. Safarzadeh, E. Berger, K. K. Y. Ng, H.-Y. Chen, S. Vitale, C. Whittle, and E. Scannapieco, Astrophys. J. Lett. **878**, L13 (2019).

[37] K. S. McCarthy, Z. Zheng, and E. Ramirez-Ruiz, Mon. Not. R. Astron. Soc. **499**, 5220 (2020).

[38] L. Greggio, P. Simonetti, and F. Matteucci, Mon. Not. R. Astron. Soc. **500**, 1755 (2020).

[39] V. Takhistov, G. M. Fuller, and A. Kusenko, Phys. Rev. Lett. **126**, 071101 (2021).

[40] B. Dasgupta, R. Laha, and A. Ray, Phys. Rev. Lett. **126**, 141105 (2021).

[41] C. D. Bailyn, R. K. Jain, P. Coppi, and J. A. Orosz, Astrophys. J. **499**, 367 (1998).

[42] F. Özel, D. Psaltis, R. Narayan, and J. E. McClintock, Astrophys. J. **725,** 1918 (2010).

[43] W. M. Farr, N. Sravan, A. Cantrell, L. Kreidberg, C. D. Bailyn, I. Mandel, and V. Kalogera, Astrophys. J. **741,** 103 (2011).

[44] K. Belczynski, G. Wiktorowicz, C. L. Fryer, D. E. Holz, and V. Kalogera, Astrophys. J. **757,** 91 (2012).

[45] C. L. Fryer, A. Olejak, and K. Belczynski, Astrophys. J. **931,** 94 (2022).

[46] V. De Luca, G. Franciolini, P. Pani, and A. Riotto, Phys. Rev. D **102,** 043505 (2020).

[47] D. Gerosa, E. Berti, R. O'Shaughnessy, K. Belczynski, M. Kesden, D. Wysocki, and W. Gladysz, Phys. Rev. D **98,** 084036 (2018).

[48] K. Belczynski *et al.*, Astron. Astrophys. **636,** A104 (2020).

[49] G. Franciolini, R. Cotesta, N. Loutrel, E. Berti, P. Pani, and A. Riotto, Phys. Rev. D **105,** 063510 (2022).

[50] S. Mukherjee and J. Silk, Mon. Not. R. Astron. Soc. **506,** 3977 (2021).

[51] S. Mukherjee, M. S. P. Meinema, and J. Silk, Mon. Not. R. Astron. Soc. **510,** 6218 (2022).

[52] C. J. Hansen and S. D. Kawaler, *Stellar Interiors: Physical Principles, Structure, and Evolution* (Springer, New York, NY, 1994).

[53] G. Chabrier, Astrophys. Space Sci. Libr. **327,** 41 (2005).

[54] T. Damour, in *300 Years of Gravity: A Conference to Mark the 300th Anniversary of the Publication of Newton's Principia* (1986).

[55] T. Mora and C. M. Will, Phys. Rev. D **69,** 104021 (2004); **71,** 129901(E) (2005).

[56] T. Damour and A. Nagar, Phys. Rev. D **80,** 084035 (2009).

[57] P. Landry and E. Poisson, Phys. Rev. D **91,** 104018 (2015).

[58] H. S. Chia, Phys. Rev. D **104,** 024013 (2021).

[59] E. Poisson, Phys. Rev. D **104,** 104062 (2021).

[60] T. Binnington and E. Poisson, Phys. Rev. D **80,** 084018 (2009).

[61] K. Chatziioannou, Gen. Relativ. Gravit. **52,** 109 (2020).

[62] T. Hinderer, B. D. Lackey, R. N. Lang, and J. S. Read, Phys. Rev. D **81,** 123016 (2010).

[63] B. P. Abbott *et al.* (LIGO Scientific and Virgo Collaborations), Classical Quantum Gravity **37,** 045006 (2020).

[64] H. Yang, W. E. East, and L. Lehner, Astrophys. J. **856,** 110 (2018); **870,** 139(E) (2019).

[65] H.-Y. Chen and K. Chatziioannou, Astrophys. J. Lett. **893,** L41 (2020).

[66] M. Fasano, K. W. K. Wong, A. Maselli, E. Berti, V. Ferrari, and B. S. Sathyaprakash, Phys. Rev. D **102,** 023025 (2020).

[67] R. N. Manchester, G. B. Hobbs, A. Teoh, and M. Hobbs, Astron. J. **129,** 1993 (2005).

[68] R. P. Breton, Radio pulsars in binary systems, Ph.D. thesis, McGill University, 2008, arXiv:0907.2623.

[69] P. C. Peters and J. Mathews, Phys. Rev. **131,** 435 (1963).

[70] B. S. Sathyaprakash and S. V. Dhurandhar, Phys. Rev. D **44,** 3819 (1991).

[71] B. S. Sathyaprakash and B. F. Schutz, Living Rev. Relativity **12,** 2 (2009).

[72] E. E. Flanagan and T. Hinderer, Phys. Rev. D **77,** 021502 (2008).

[73] M. Favata, Phys. Rev. Lett. **112,** 101101 (2014).

[74] S. De, D. Finstad, J. M. Lattimer, D. A. Brown, E. Berger, and C. M. Biwer, Phys. Rev. Lett. **121,** 091102 (2018); **121,** 259902(E) (2018).

[75] B. P. Abbott *et al.* (LIGO Scientific and Virgo Collaborations), Phys. Rev. Lett. **121,** 161101 (2018).

[76] N. K. Johnson-Mcdaniel, A. Mukherjee, R. Kashyap, P. Ajith, W. Del Pozzo, and S. Vitale, Phys. Rev. D **102,** 123010 (2020).

[77] A. Chen, N. K. Johnson-McDaniel, T. Dietrich, and R. Dudi, Phys. Rev. D **101,** 103008 (2020).

[78] L. S. Finn, Phys. Rev. D **46,** 5236 (1992).

[79] M. Vallisneri, Phys. Rev. D **77,** 042001 (2008).

[80] S. Borhanian, Classical Quantum Gravity **38,** 175014 (2021).

[81] B. P. Abbott *et al.* (LIGO Scientific and Virgo Collaborations), Phys. Rev. Lett. **119,** 161101 (2017).

[82] B. P. Abbott *et al.* (LIGO Scientific and Virgo Collaborations), Phys. Rev. X **9,** 011001 (2019).

[83] D. Radice, A. Perego, F. Zappa, and S. Bernuzzi, Astrophys. J. Lett. **852,** L29 (2018).

[84] B. P. Abbott *et al.* (LIGO Scientific and Virgo Collaborations), Astrophys. J. Lett. **892,** L3 (2020).

[85] D. Reitze *et al.*, Bull. Am. Astron. Soc. **51,** 035 (2019), arXiv:1907.04833.

[86] M. Punturo *et al.*, Classical Quantum Gravity **27,** 084007 (2010).

[87] L. Barsotti, L. McCuller, M.Evans, and P. Fritschel, The A+ design curve, LIGO (2018), https://dcc.ligo.org/LIGO-T1800042/public.

[88] R. X. Adhikari *et al.*, Classical Quantum Gravity **36,** 245010 (2019).

[89] T. Dietrich, S. Bernuzzi, and W. Tichy, Phys. Rev. D **96,** 121501 (2017).

[90] T. Dietrich *et al.*, Phys. Rev. D **99,** 024029 (2019).

[91] T. Dietrich, A. Samajdar, S. Khan, N. K. Johnson-McDaniel, R. Dudi, and W. Tichy, Phys. Rev. D **100,** 044003 (2019).

[92] K. D. Kokkotas and G. Schaefer, Mon. Not. R. Astron. Soc. **275,** 301 (1995).

[93] L. Gualtieri, E. Berti, J. A. Pons, G. Miniutti, and V. Ferrari, Phys. Rev. D **64,** 104007 (2001).

[94] J. A. Pons, E. Berti, L. Gualtieri, G. Miniutti, and V. Ferrari, Phys. Rev. D **65,** 104021 (2002).

[95] E. Berti, J. A. Pons, G. Miniutti, L. Gualtieri, and V. Ferrari, Phys. Rev. D **66,** 064013 (2002).

[96] J. Steinhoff, T. Hinderer, A. Buonanno, and A. Taracchini, Phys. Rev. D **94,** 104028 (2016).

[97] N. Andersson and P. Pnigouras, Mon. Not. R. Astron. Soc. **503,** 533 (2021).

[98] P. Schmidt and T. Hinderer, Phys. Rev. D **100,** 021501 (2019).

[99] G. Pratten, P. Schmidt, and N. Williams, Phys. Rev. Lett. **129,** 081102 (2022).

[100] R. Gamba and S. Bernuzzi, Phys. Rev. D **107,** 044014 (2023).

[101] N. Williams, G. Pratten, and P. Schmidt, Phys. Rev. D **105,** 123032 (2022).

[102] B. Kiziltan, A. Kottas, M. De Yoreo, and S. E. Thorsett, Astrophys. J. **778,** 66 (2013).

[103] N. Farrow, X.-J. Zhu, and E. Thrane, Astrophys. J. **876**, 18 (2019).

[104] P. Landry and J. S. Read, Astrophys. J. Lett. **921**, L25 (2021).

[105] R. Abbott *et al.* (LIGO Scientific, VIRGO, and KAGRA Collaborations), Phys. Rev. X **13**, 011048 (2023).

[106] M. Dominik, K. Belczynski, C. Fryer, D. E. Holz, E. Berti, T. Bulik, I. Mandel, and R. O'Shaughnessy, Astrophys. J. **779**, 72 (2013).

[107] M. Dominik, E. Berti, R. O'Shaughnessy, I. Mandel, K. Belczynski, C. Fryer, D. E. Holz, T. Bulik, and F. Pannarale, Astrophys. J. **806**, 263 (2015).

[108] F. Santoliquido, M. Mapelli, N. Giacobbo, Y. Bouffanais, and M. C. Artale, Mon. Not. R. Astron. Soc. **502**, 4877 (2021).

[109] P. Madau and M. Dickinson, Annu. Rev. Astron. Astrophys. **52**, 415 (2014).

[110] V. Sahni and A. A. Starobinsky, Int. J. Mod. Phys. D **09**, 373 (2000).

[111] C. T. Byrnes, M. Hindmarsh, S. Young, and M. R. S. Hawkins, J. Cosmol. Astropart. Phys. 08 (2018) 041.

[112] R. Abbott *et al.* (LIGO Scientific, VIRGO, and KAGRA Collaborations), Phys. Rev. Lett. **129**, 061104 (2022).

[113] W. H. Press and D. N. Spergel, Astrophys. J. **296**, 679 (1985).

[114] A. Gould, Astrophys. J. **321**, 571 (1987).

[115] S. D. McDermott, H.-B. Yu, and K. M. Zurek, Phys. Rev. D **85**, 023519 (2012).

[116] R. Garani, Y. Genolini, and T. Hambye, J. Cosmol. Astropart. Phys. 05 (2019) 035.

[117] N. F. Bell, G. Busoni, S. Robles, and M. Virgato, J. Cosmol. Astropart. Phys. 09 (2020) 028.

[118] N. F. Bell, G. Busoni, T. F. Motta, S. Robles, A. W. Thomas, and M. Virgato, Phys. Rev. Lett. **127**, 111803 (2021).

[119] F. Anzuini, N. F. Bell, G. Busoni, T. F. Motta, S. Robles, A. W. Thomas, and M. Virgato, J. Cosmol. Astropart. Phys. 11 (2021) 056.

[120] B. Bertoni, A. E. Nelson, and S. Reddy, Phys. Rev. D **88**, 123505 (2013).

[121] R. Garani, A. Gupta, and N. Raj, Phys. Rev. D **103**, 043019 (2021).

[122] C. Kouvaris and P. Tinyakov, Phys. Rev. Lett. **107**, 091301 (2011).

[123] W. E. East and L. Lehner, Phys. Rev. D **100**, 124026 (2019).

[124] T. W. Baumgarte and S. L. Shapiro, Phys. Rev. D **103**, L081303 (2021).

[125] C. B. Richards, T. W. Baumgarte, and S. L. Shapiro, Phys. Rev. D **103**, 104009 (2021).

[126] C. B. Richards, T. W. Baumgarte, and S. L. Shapiro, Mon. Not. R. Astron. Soc. **502**, 3003 (2021).

[127] A. Aguayo-Ortiz, E. Tejeda, O. Sarbach, and D. López-Cámara, Mon. Not. R. Astron. Soc. **504**, 5039 (2021).

[128] P. Giffin, J. Lloyd, S. D. McDermott, and S. Profumo, Phys. Rev. D **105**, 123030 (2022).

[129] J. Aalbers *et al.* (LZ Collaboration), arXiv:2207.03764.

[130] P. Agnes *et al.* (DarkSide-50 Collaboration), Phys. Rev. D **107**, 063001 (2023).

[131] E. Aprile *et al.* (XENON Collaboration), Phys. Rev. Lett. **129**, 161805 (2022).

[132] L. Barak *et al.* (SENSEI Collaboration), Phys. Rev. Lett. **125**, 171802 (2020).

[133] E. Aprile *et al.* (XENON Collaboration), Phys. Rev. Lett. **121**, 111302 (2018).

[134] R. A. Allsman *et al.* (Macho Collaboration), Astrophys. J. Lett. **550**, L169 (2001).

[135] P. Tisserand *et al.* (EROS-2 Collaboration), Astron. Astrophys. **469**, 387 (2007).

[136] L. Wyrzykowski, J. Skowron, S. Kozłowski, A. Udalski, M. K. Szymański, M. Kubiak, G. Pietrzyński, I. Soszyński, O. Szewczyk, K. Ulaczyk, R. Poleski, and P. Tisserand, Mon. Not. R. Astron. Soc. **416**, 2949 (2011).

[137] S. M. Koushiappas and A. Loeb, Phys. Rev. Lett. **119**, 041102 (2017).

[138] B. Abbott *et al.* (LIGO Scientific Collaboration), Phys. Rev. D **72**, 082002 (2005).